International Journal of Modern Physics A
Vol. 30, No. 6 (2015) 1541002 (44 pages)

DOI: 10.1142/S0217751X1541002X

World Scientific
www.worldscientific.com

Review of physics results from the Tevatron: QCD physics

Christina Mesropian

The Rockefeller University,
Laboratory of Experimental High Energy Physics,
1230 York Avenue, NY 10065, USA
christina.mesropian@rockefeller.edu

Dmitry Bandurin

Department of Physics, University of Virginia,
Charlottesville, Virginia 22904, USA
bandurin@fnal.gov

Received 17 September 2014
Published 17 February 2015

We present a summary of results from studies of quantum chromodynamics at the Fermilab Tevatron collider by the CDF and the D0 experiments. These include Run II results for the time period up to the end of Summer 2014. A brief description of Run I results is also given. This review covers a wide spectrum of topics, and includes measurements with jet and vector boson final states in the hard (perturbative) energy regime, as well as studies of soft physics such as diffractive and elastic scatterings, underlying and minimum bias events, hadron fragmentation, and multiple parton interactions.

Keywords: Quantum chromodynamics; hadron jet; direct photons; strong coupling; parton density functions; diffraction; elastic scattering; hadron fragmentation; multiple parton interactions.

PACS numbers: 13.87.Ce, 13.85.Qk, 12.38.Qk, 14.70.Fm, 24.10.Ht, 12.40.Nn

Contents

1. Introduction 2
2. Summary of Run I Results 3
3. Jet Final States 4
   3.1. Measurements of multijet cross-sections 4
   3.2. Extraction of α_s 10
   3.3. Jet substructure 11
   3.4. Jet shapes 12
   3.5. New phenomena searches 13

4. Photon Final States 14
4.1. Inclusive photon production 14
4.2. Photon + jet production 15
4.3. Photon + heavy flavor jet production 17
4.4. Diphoton production 18
5. W/Z + Jets Final States 20
5.1. W/Z + jet production 20
5.2. W/Z + heavy flavor jet production 22
6. Soft QCD 24
6.1. Nondiffractive production 25
6.1.1. Minimum bias studies 25
6.1.2. Underlying event studies 26
6.1.3. Particle production 28
6.1.4. Fragmentation studies 29
6.1.5. Event shapes 30
6.2. Elastic scattering 31
6.3. Diffractive processes 32
6.3.1. Hard single diffraction 33
6.3.2. Central exclusive production 34
6.4. Study of double parton interactions 37
7. Summary and Conclusions 39

1. Introduction

Quantum chromodynamics (QCD) is the theory of interacting quarks and gluons, which are the fundamental constituents of hadrons. QCD achieved remarkable success in describing the strong interaction processes at hadron colliders at short distances, i.e. large momentum transfers, by applying well developed perturbative techniques. However, QCD still lacks good understanding of quark–gluon interactions at large distances, or low moment transfers, mostly due to the mathematical complexity of the theory and the nonapplicability of perturbative methods at this range.

QCD studies at the Tevatron contributed significantly to the major progress in understanding the strong interactions. In this section, we describe QCD measurements performed by the CDF and D0 collaborations at the Fermilab Run II Tevatron $p\bar{p}$ collider using data collected at center-of-mass energy $\sqrt{s} = 1.96\,\text{TeV}$. They address various aspects of QCD theory, providing rigorous tests of predictions for hadron colliders, and guiding priorities to reduce uncertainties for the most problematic parts of the theory.

We start our review with a brief summary of Run I physics results, obtained at $\sqrt{s} = 0.63$ and $1.8\,\text{TeV}$, in Sec. 2.

In Sec. 3, we present the inclusive jet, dijet production and three-jet cross-section measurements which are used to test perturbative QCD (pQCD) calculations, constrain parton distribution functions (PDFs), and extract a precise value of the strong coupling constant α_s. They are also used to search for new phenomena expected at high energies.

Section 4 describes measurements with photon final states. Inclusive photon (γ) and $\gamma +$ jet production cross-section measurements provide information for tuning QCD theory predictions and particularly can be used as a direct constraint for global fits to gluon and other PDFs. The diphoton production cross-sections check the validity of next-to-leading-order (NLO) pQCD predictions, soft-gluon resummation methods implemented in theoretical calculations, and contributions from the parton-to-photon fragmentation diagrams.

Events with $W/Z +$ jets productions are used to measure many kinematic distributions allowing extensive tests and tunes of predictions from pQCD NLO and Monte Carlo event generators. They are discussed in Sec. 5.

All previously mentioned measurements belong to the processes that can be treated in the framework of perturbative QCD. The majority of hadron–hadron collision processes are related to the general unsolved problems of soft strong interactions, and their studies are discussed in Sec. 6. The charged-particle transverse momenta (p_T) and multiplicity distributions in inclusive minimum bias events are used to tune nonperturbative QCD models, including those describing multiple parton interactions (MPI). Events with inclusive production of γ and 2 or 3 jets are used to study increasingly important MPI phenomenon at high p_T, measure an effective interaction cross-section, allowing the prediction of rates of double parton interactions, and providing constraints for existing MPI models. The study of characteristics of soft particle production enables us to differentiate between various approaches describing hadronization. Elastic scattering $p\bar{p} \to p\bar{p}$ is an important process that probes the structure of the proton. Study of diffractive processes is an important source in understanding many interesting aspects of QCD such as low-x structure of the proton and the behavior of QCD in the high density regime, and provides an ultimate approach in understanding nonperturbative QCD.

We summarize our results in Sec. 7.

2. Summary of Run I Results

With the increased luminosity performance of the Tevatron in Run I, when each experiment collected around $20\,\mathrm{pb}^{-1}$ of data in 1992–1993 (Run 1A) and $100\,\mathrm{pb}^{-1}$ of data in 1994–1996 (Run 1B) with a small data sample of $600\,\mathrm{nb}^{-1}$ being collected at $\sqrt{s} = 630\,\mathrm{GeV}$, the new era of precision $p\bar{p}$ QCD measurements began.

The cross-section measurements for inclusive jet and dijet production (see Sec. 3) were no longer limited by statistical uncertainties and resulting systematic uncertainties were comparable to uncertainties from theoretical predictions. This improvement revealed significant flexibility in parton distribution functions, especially for large x gluons, and motivated inclusion of the Tevatron jet data in the

global PDF analyses to constrain gluon distributions,[1] thus making predictions more precise, particularly in processes where gluon–quark scattering dominates.

QCD predictions were tested further by comparing with the measurements of the ratio of inclusive jet cross-sections at $\sqrt{s} = 630$ and 1800 GeV, dijet cross-sections at large rapidity, and a set of photon and photon + jet final state measurements (see Sec. 4) for both $\sqrt{s} = 1800$ GeV and $\sqrt{s} = 630$ GeV. The strong coupling constant, a free parameter of QCD, was measured from inclusive jet production, and its *running* was tested on a wide range of momentum transfers. The groundwork for extensive Run II studies of W/Z + jet final states (see Sec. 5) was laid by measurements of the cross-sections and the properties of vector boson production in association with jets.

The soft strong interactions were studied in detail by measuring charged particle distributions, developing new approaches for studies of the underlying event, and measuring the effective cross-section in events with the multi-parton interactions (Sec. 6).

Legacy of Run I diffractive measurements were observations of rapidity gaps between two jets, many observations regarding the diffractive structure function of the pomeron, and the breakdown of QCD factorization in hard diffraction between Tevatron and HERA.

3. Jet Final States

3.1. *Measurements of multijet cross-sections*

Stringent tests of NLO pQCD were obtained from the study of final states with high E_T jets: inclusive jet and dijet differential cross-sections, dijet mass, dijet angular and multijet distributions. The Run II data provide a thorough testing of pQCD theory predictions at short distances through measurements of differential inclusive jet, dijet and three-jet cross-sections. Both experiments measured the inclusive jet cross-sections as a function of jet transverse momentum p_T in several rapidity y regions. The D0 collaboration measured cross-section using jets found by the Midpoint cone algorithm[2] with radius $R = 0.7$ for transverse momenta from 50 GeV to 600 GeV and jet rapidities in the range -2.4 to 2.4. Figure 1 shows the differential cross-section ($d^2\sigma/dp_T dy$) measured by D0 collaboration,[3] and Fig. 2 shows a ratio of the measured cross-section to NLO pQCD predictions. Figure 3 shows a similar ratio for the jet cross-sections measured by the CDF collaboration[4] up to $|y| < 2.1$. (Similar measurements of the inclusive jet cross-section have been made by the CDF collaboration using the k_T jet clustering algorithm.[5]) Both measurements are in agreement with pQCD predictions. However, data with uncertainties smaller than those from theoretical calculations (mostly from PDF), favor a smaller gluon content at high parton momentum fractions x ($x > 0.2$). The jet measurements, being dominated by systematic uncertainties, are performed using data with 0.4–1 fb^{-1} of integrated luminosity.

Figure 4 presents a measurement of the dijet production cross-section as a function of the dijet invariant mass and of the largest rapidity of the two highest p_T

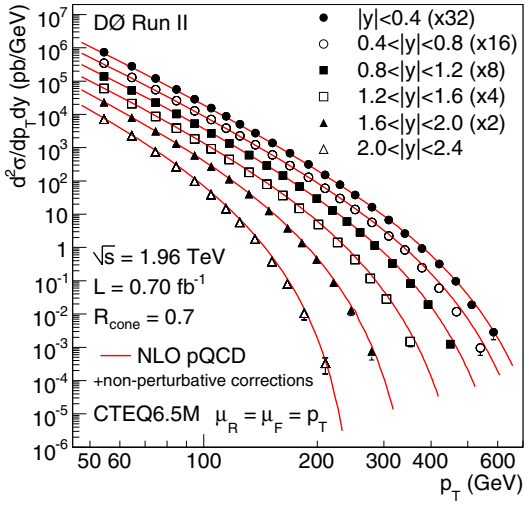

Fig. 1. The inclusive jet cross-section as a function of jet p_T in six rapidity $|y|$ bins. The data points are multiplied by 2, 4, 8, 16 and 32 for the bins $1.6 < |y| < 2.0$, $1.2 < |y| < 1.6$, $0.8 < |y| < 1.2$, $0.4 < |y| < 0.8$ and $|y| < 0.4$, respectively.

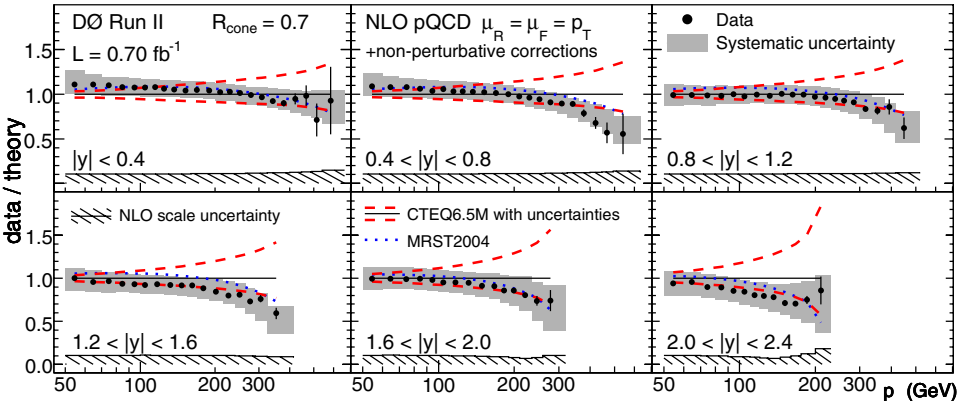

Fig. 2. Measured data divided by theory predictions. The data systematic uncertainties are displayed by the full shaded band. NLO pQCD calculations, with renormalization and factorization scales set to jet pT using the CTEQ6.5M PDFs and including nonperturbative corrections, are compared to the data. The CTEQ6.5 PDF uncertainties are shown as dashed lines and the predictions with MRST2004 PDFs as dotted lines. The theoretical uncertainty, determined by changing the renormalization and factorization scales between $p_T/2$ and $2p_T$, is shown at the bottom of each figure.

jets.[6] The data are described by NLO pQCD predictions using MSTW2008NLO[7] PDFs in all rapidity regions, and are not well described by CTEQ6.6 PDF,[8] particularly at high jet rapidities.

The differential cross-section in the three-jet invariant mass ($M_{3\text{jet}}$) is measured by the D0 collaboration in five scenarios, spanning different rapidity regions and

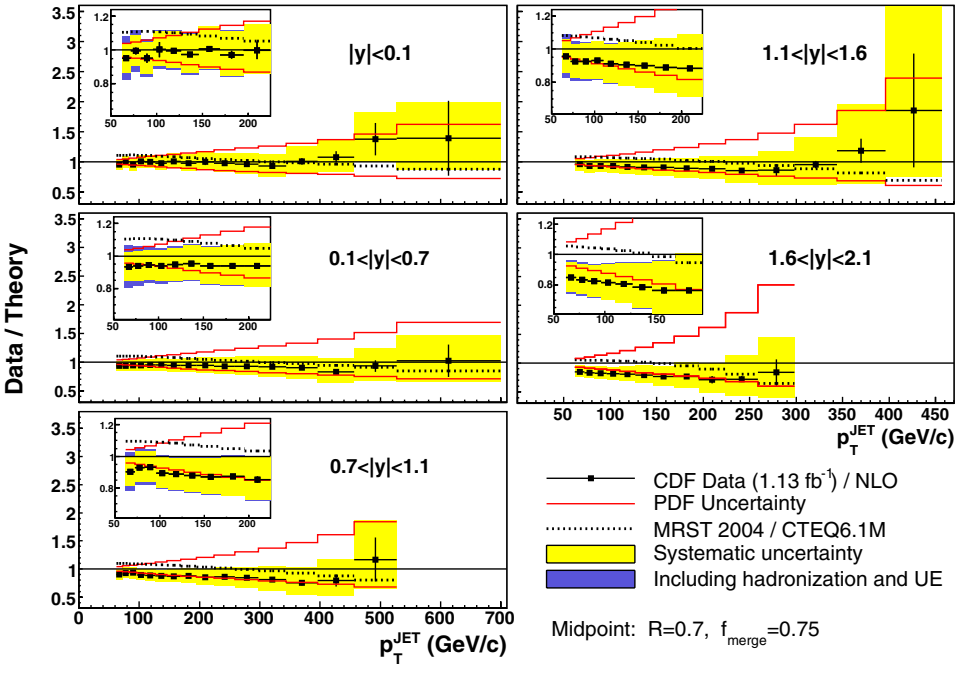

Fig. 3. The ratios of the measured inclusive jet cross-sections at the hadron level with the Midpoint jet clustering algorithm to the NLO pQCD predictions (corrected to the hadron level) in five rapidity regions. Also shown are the experimental systematic uncertainties on the measured cross-section, the uncertainties in the hadronization and underlying event corrections added in quadrature with the experimental systematic uncertainties, and the PDF uncertainties on the theoretical predictions.

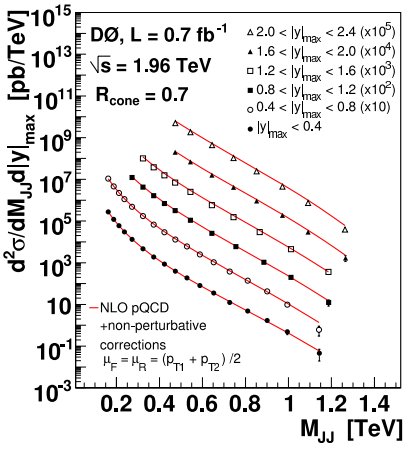

Fig. 4. The dijet production cross-section as a function of invariant mass in intervals of $|y|_{\max}$ compared to NLO predictions that include nonperturbative corrections. Uncertainties shown are statistical only.

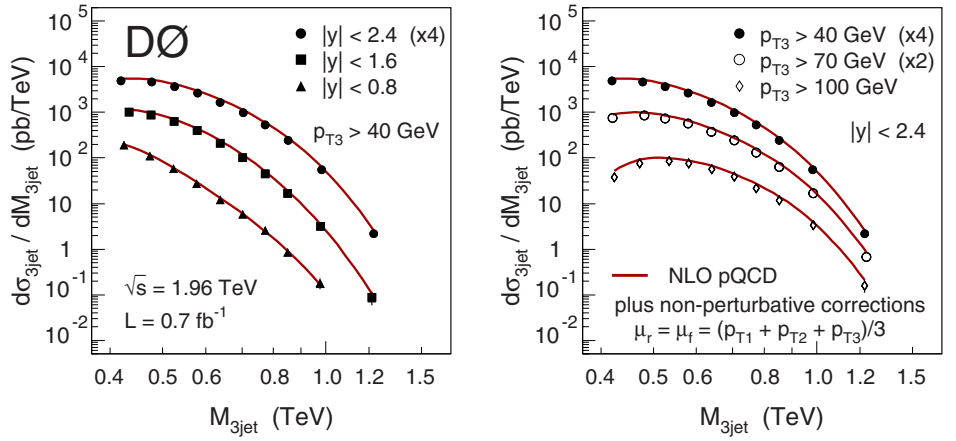

(a) (b)

Fig. 5. The differential cross-section $d\sigma_{3\text{jet}}/dM_{3\text{jet}}$ (a) in different rapidity regions and (b) for different p_{T3} requirements. The solid lines represent the NLO pQCD matrix element calculations using MSTW2008NLO PDFs and $\alpha_s(M_Z) = 0.1202$ which are corrected for nonperturbative effects.

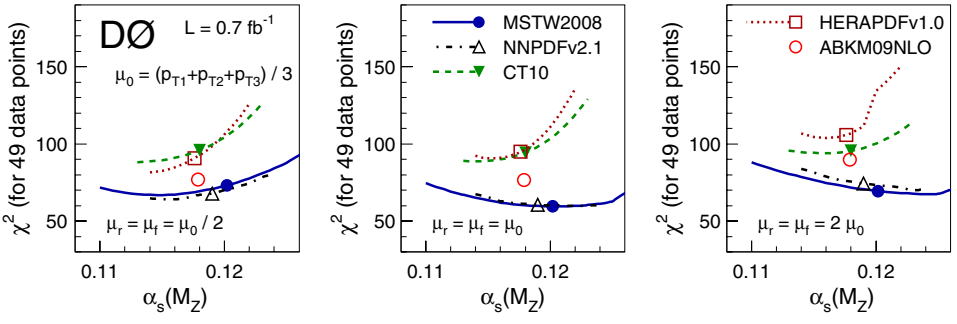

(a) (b) (c)

Fig. 6. The χ^2 values between theory and data, as a function of the value of $\alpha_s(M_Z)$ used in the matrix elements and PDFs. The results are shown for different PDF parametrizations and for different choices of the renormalization and factorization scales. The positions of the central $\alpha_s(M_Z)$ values in the different PDF sets are indicated by the markers.

for different requirements on the jet transverse momenta (see Fig. 5).[9] Jets are ordered in descending p_T with the requirements $p_{T1} > 150\,\text{GeV}$ and $p_{T3} > 40\,\text{GeV}$ (and no further requirement on p_{T2}). The rapidities of the three leading p_T jets are restricted to $|y| < 0.8$, $|y| < 1.6$, or $|y| < 2.4$, in three different measurements. Two additional measurements are made for $p_{T3} > 70\,\text{GeV}$ and $p_{T3} > 100\,\text{GeV}$, both requiring $|y| < 2.4$. The data are compared to pQCD calculations at NLO in α_s for different PDF parametrizations, by computing χ^2 values for different scale choices and different $\alpha_s(M_Z)$ values (see Fig. 6). The best description of the data is

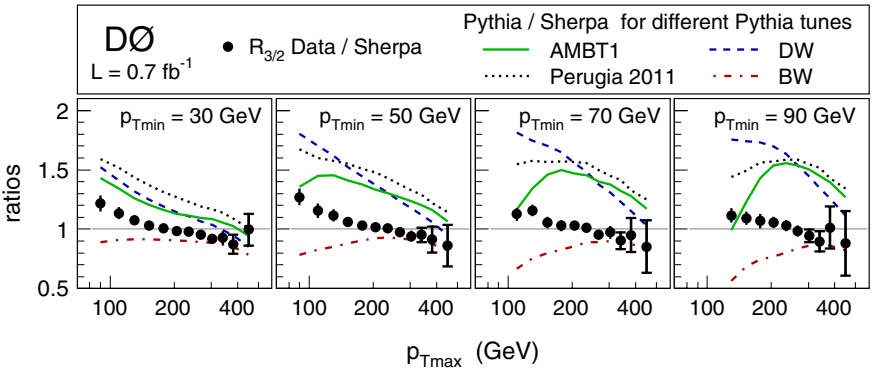

Fig. 7. The measured $R_{3/2}$ results, normalized to the predictions of the SHERPA Monte Carlo event generator. The inner uncertainty bars represent the statistical uncertainties while the total uncertainty bars represent the quadratic sums of statistical and systematic uncertainties. Overlaid are the predictions from the PYTHIA Monte Carlo event generator for four different tunes, also normalized to the SHERPA predictions.

obtained for the MSTW2008NLO[7] and NNPDFv2.1[10] PDF parametrizations which describe both the normalization and the shape of the observed $M_{3\text{jet}}$ spectra. The PDF parametrizations from ABKM09NLO[11] give a reasonable description of the data, although with a slightly different shape of the $M_{3\text{jet}}$ spectrum. The central results from the CT10[12] and HERAPDFv1.0 PDF[13] sets predict a different $M_{3\text{jet}}$ shape and are in poorer agreement with the data.

The ratio of three-jet to two-jet cross-sections ($R_{3/2}$) has also been measured.[14] The ratio $R_{3/2}$ is presented in Fig. 7 for the minimum jet p_T ($p_{T\min}$) requirements of 30, 50, 70 and 90 GeV, as a function of the highest jet p_T ($p_{T\max}$) in the range of 80–500 GeV. The SHERPA event generator[15] describes the data within approximately -10% to $+20\%$, but predicts a slightly different $p_{T\max}$ dependence. None of the PYTHIA MPI tunes DW, BW, A, AMBT1, S Global, and Perugia 2011[16] describes the data. The data are well described by the pQCD predictions at NLO in α_s, corrected for nonperturbative effects estimated from hadronization and underlying event corrections using PYTHIAtunes DW and AMBT1.

Multi-parton radiation is a complex aspect of pQCD theory and related phenomenology. The proper description of radiative processes is crucial for a wide range of precision measurements as well as for searches for new phenomena where the influence of QCD radiation is unavoidable. A clean and simple way to study radiative processes is to examine azimuthal decorrelations in dijet events. Results from HERWIG (version 6.505) and PYTHIA (version 6.225) Monte Carlo generators, both using default parameters and the CTEQ6L[8] PDFs, are compared to the $\Delta\phi_{\text{dijet}}$ measurement in the events with at least two jets[17] in Fig. 8. The minimum jet p_T, $p_{T\min}$, is 40 GeV while $p_{T\max}$ is varied. The data are described by HERWIG well over the entire $\Delta\phi_{\text{dijet}}$ range including the region around $\Delta\phi_{\text{dijet}} \approx \pi$. PYTHIA with default parameters describes the data poorly — the distribution is too narrowly

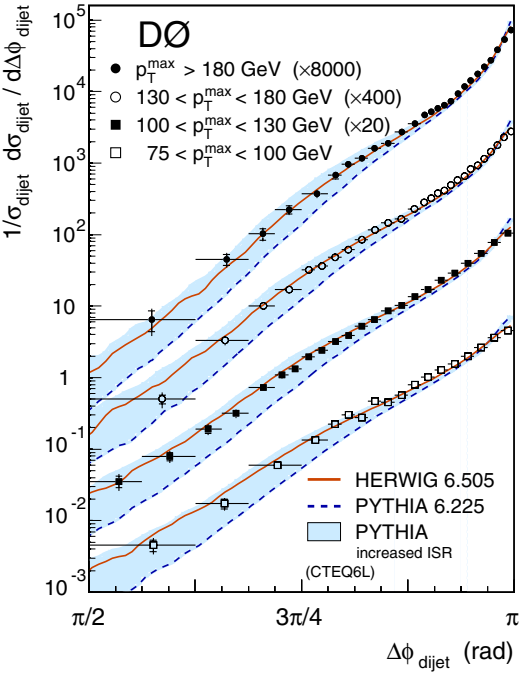

Fig. 8. The $\Delta\phi_{\,\mathrm{dijet}}$ distributions in different $p_{T\max}$ ranges. Results from HERWIG and PYTHIA are overlaid on the data. Data and predictions with $p_{T\max} > 100\,\mathrm{GeV}$ are scaled by successive factors of 20 for purposes of presentation.

peaked at $\Delta\phi_{\,\mathrm{dijet}} \approx \pi$ and lies significantly below the data over most of the $\Delta\phi_{\,\mathrm{dijet}}$ range. The maximum p_T in the initial-state parton shower is directly related to the maximum virtuality that can be adjusted in PYTHIA. The shaded bands indicate the range of variation when the maximum allowed virtuality is increased from the current default by a factor of four.[18] These variations result in significant changes in the low $\Delta\phi_{\,\mathrm{dijet}}$ region clearly demonstrating the sensitivity of this measurement. Consequently, global efforts to tune Monte Carlo event generators should benefit from including these data. NLO pQCD describes the data except for very large $\Delta\phi_{\,\mathrm{dijet}}$ where the calculation does not provide a reliable prediction.

The combined rapidity and p_T dependence of dijet azimuthal decorrelations has also been studied.[19] This measurement is based on a new quantity $R_{\Delta\phi}$, defined as the fraction of the inclusive dijet cross-section with a decorrelation of $\Delta\phi_{\,\mathrm{dijet}} < \Delta\phi_{\max}$. The ratio $R_{\Delta\phi}$ is measured as a function of the total jet transverse momentum H_T, the rapidity $y^* = |y_{\mathrm{jet1}} - y_{\mathrm{jet2}}|$, and the maximal azimuthal decorrelation with $\Delta\phi_{\max}$, see Fig. 9. For all values of $\Delta\phi_{\max}$ and at fixed H_T, dijet azimuthal decorrelations increase with y^*, while they decrease with H_T over most of the H_T range at fixed y^*. Predictions of NLO pQCD, corrected for nonperturbative effects, give a good description of the data, except in the kinematic region of large dijet rapidity intervals $y^* > 1$ and small decorrelations with $\Delta\phi_{\max} = 7\pi/8$.

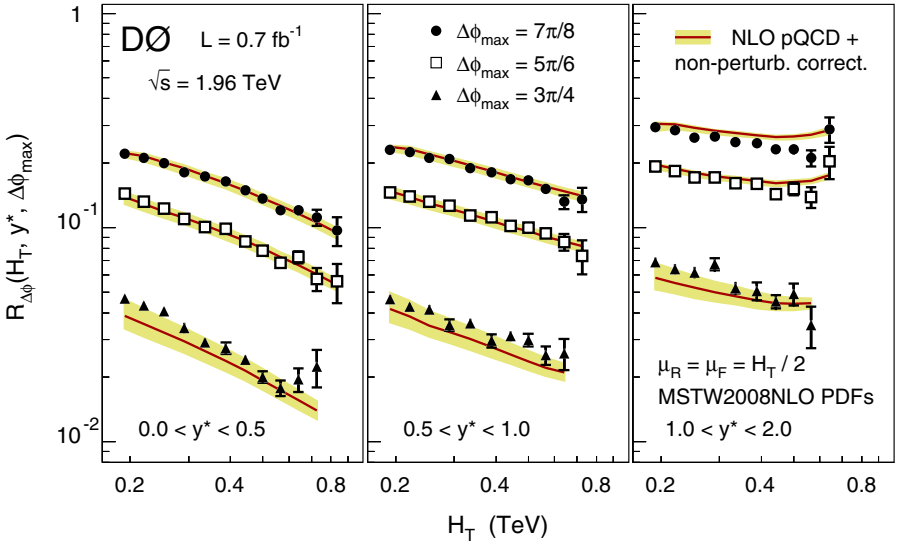

Fig. 9. The results for $R_{\Delta\phi}$ as a function of H_T in three different regions of y^* and for three different $\Delta\phi_{\max}$ requirements. The error bars indicate the statistical and systematic uncertainties summed in quadrature. The theoretical predictions are shown with their uncertainties.

3.2. *Extraction of α_s*

The D0 inclusive jet data has been used to extract values of the strong coupling constant α_s in the interval of $50 < p_T^{\text{jet}} < 145\,\text{GeV}$.[20] The best fit over 22 data points leads to $\alpha_s(m_Z) = 0.1161^{+0.0041}_{-0.0048}$ with improved accuracy as compared to the Run I CDF result,[21] $\alpha_s(m_Z) = 0.1178^{+0.0122}_{-0.0121}$, and also in agreement with result from HERA jet data.[22]

A new quantity $R_{\Delta R}$ which probes the angular correlations of jets has been introduced.[23] It is defined as the number of neighboring jets above a given transverse momentum threshold which accompany a given jet within a given distance ΔR in the plane of rapidity and azimuthal angle. $R_{\Delta R}$ is measured as a function of inclusive jet p_T in different annular regions of ΔR between a jet and its neighboring jets and for different requirements on the minimal transverse momentum of the neighboring jet $p_{T\min}^{\text{nbr}}$ (see Fig. 10). The data for $p_T > 50\,\text{GeV}$ are well-described by pQCD calculations in NLO in α_s with nonperturbative corrections applied. Results for $\alpha_s(p_T)$ are extracted using the data with $p_{T\min}^{\text{nbr}} \geq 50\,\text{GeV}$, integrated over ΔR. The extracted $\alpha_s(p_T)$ results from $R_{\Delta R}$ are, to good approximation, independent of the PDFs and thus independent of assumptions on the renormalization group equation (RGE). The results are in good agreement with previous results and consistent with the RGE predictions for the running of α_s for momentum transfers up to 400 GeV (see Fig. 11). The combined $\alpha_s(M_Z)$ result, integrated over ΔR and p_T, is $\alpha_s(M_Z) = 0.1191^{+0.0048}_{-0.0071}$, in good agreement with the world average value.[24]

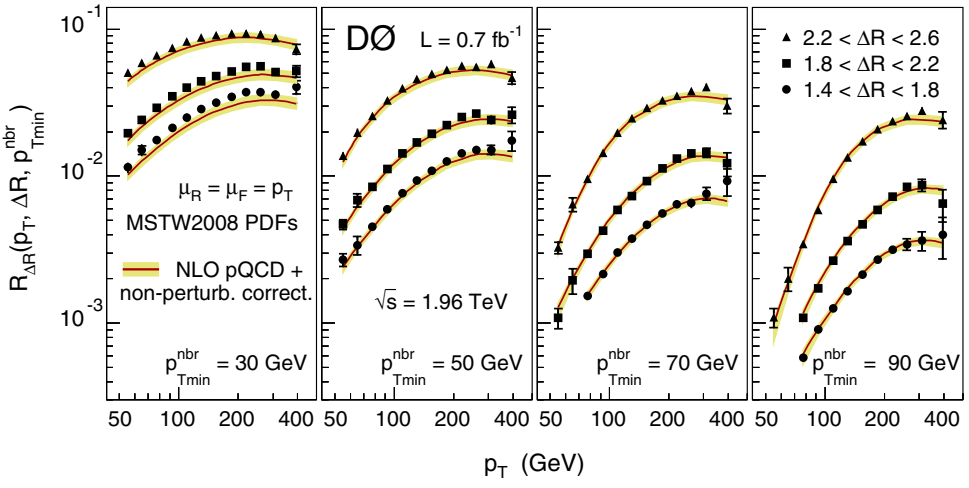

Fig. 10. The measurement of $R_{\Delta R}$ as a function of inclusive jet p_T for three different intervals in ΔR and for four different requirements of $p_{T\mathrm{min}}^{\mathrm{nbr}}$. The inner uncertainty bars indicate the statistical uncertainties, and the total uncertainty bars display the quadratic sum of the statistical and systematic uncertainties. The theory predictions are shown with their uncertainties.

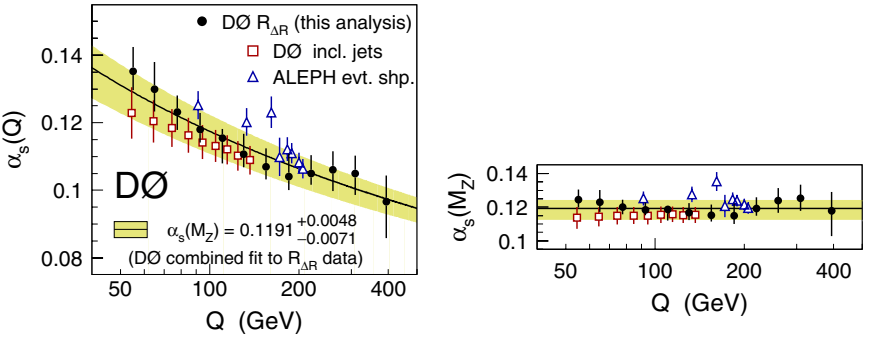

(a) (b)

Fig. 11. The strong coupling α_s at large momentum transfers, Q, presented as $\alpha_s(Q)$ (a) and evolved to M_Z using the RGE (b). The uncertainty bars indicate the total uncertainty, including the experimental and theoretical contributions. The new α_s results from $R_{\Delta R}$ are compared to previous results obtained from inclusive jet cross-section data[20] and from event shape data.[25] The $\alpha_s(M_Z)$ result from the combined fit to all selected data points (b) and the corresponding RGE prediction (a) are also shown.

3.3. *Jet substructure*

Studying the jet substructure allows for tuning parton showering and search for heavy resonances decaying hadronically and separated by a small angle. It has been one of important topics of Run I jet program (see e.g. Ref. 26).

In Run II, the CDF collaboration studied structure of high p_T jets by selecting only events with at least one jet having $p_T > 400\,\mathrm{GeV}$, $0.1 < |y| < 0.7$ and

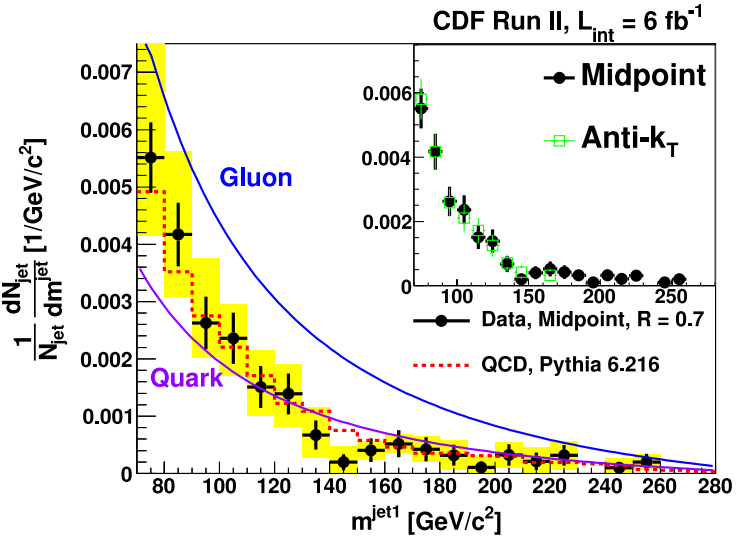

Fig. 12. (Color online) The normalized jet mass distribution for jets with $p_T > 400\,\text{GeV}$ and $|\eta| \in (0.1, 0.7)$. The uncertainties shown are statistical (black lines) and systematic (yellow bars). The theory predictions for the jet function for quarks and gluons are shown as solid curves and have an estimated uncertainty of $\sim 30\%$. We also show the PYTHIA Monte Carlo prediction (red dashed line). The inset compares jets found by Midpoint (full black circles) and anti-k_T (open green squares) algorithms.

considering jets with cone sizes $R = 0.4, 0.7$ and 1.0.[27] The jet mass is calculated using 4-vectors of calorimeter towers in a jet. Special selection to remove the t-quark events have been applied. Its mass distribution unfolded to the particle level is shown in Fig. 12. The data are in agreement PYTHIA predictions and are located between the predictions for quark and gluon jets. The data confirm that the high mass jets are mostly caused by quark fragmentation.

3.4. *Jet shapes*

Jet shapes have been studied using inclusive jet production events in the kinematic region $37 < p_T^{\text{jet}} < 380\,\text{GeV}$ and $0.1 < |y^{\text{jet}}| < 0.7$ by the CDF experiment.[28] Figure 13 shows the measured fractional total p_T outside a cone of radius $r = 0.3$ around the jet axis, $1 - \Psi(0.3/R)$, as a function of p_T^{jet}. Here Ψ is defined as

$$\Psi(r) = \frac{1}{N_{\text{jet}}} \sum_{\text{jets}} \frac{p_T(0, r)}{p_T(0, R)}, \quad 0 \le r \le R. \tag{1}$$

Jets become narrower as p_T^{jet} increases which can be mainly attributed to the change in the quark- and gluon-jet mixture in the final state and the running of the strong coupling with p_T^{jet}. PYTHIA Tune A Monte Carlo predictions, which includes enhanced contributions from initial-state gluon radiation and secondary parton interactions between remnants, provides a good description of the data. HERWIG

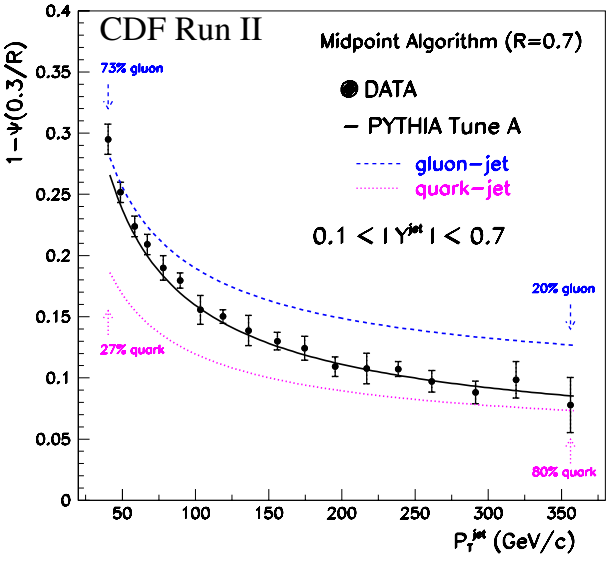

Fig. 13. The measured $1 - \Psi(0.3/R)$ as a function of p_T^{jet} for jets with $0.1 < |y^{\text{jet}}| < 0.7$ and $37 < p_T^{\text{jet}} < 380\,\text{GeV}$. Error bars indicate the statistical and systematic uncertainties added in quadrature. The predictions of PYTHIA Tune A (solid line) and the separate predictions for quark-initiated jets (dotted line) and gluon-initiated jets (dashed line) are shown for comparison. The arrows indicate the fraction of quark- and gluon-initiated jets at low and very high P_T^{jet}, as predicted by PYTHIA Tune A.

gives a reasonable description of the measured jet shapes but tends to produce jets that are too narrow at low p_T^{jet} which can be attributed to the absence of soft contributions from multiple parton interactions in HERWIG. Jet shape measurements thus can be used to introduce strong constraints on phenomenological models describing soft-gluon radiation and the underlying event in hadron–hadron interactions. Similar studies with b-jets are also done.[29]

3.5. *New phenomena searches*

The CDF collaboration performed a search for new particles which decay into dijets by measuring the dijet mass spectrum using $p\bar{p}$ collision data from $1.1\,\text{fb}^{-1}$ of integrated luminosity.[30] Since jets produced by new physics are expected to be produced more centrally than by Standard Model processes only events with two leading jets with $|y| \leq 1.0$ are used. The measured dijet mass spectrum, see Fig. 14 is found to be consistent with NLO pQCD predictions based on recent PDFs and does not show evidence of a mass resonance from new particle production. Upper limits at the 95% confidence level (CL) on new particle production cross-sections were set. The mass exclusions for the excited quark, axigluon, flavor-universal coloron, E_6 diquark, color-octet techni-ρ, W', and Z' for a specific representative set of model parameters has also been determined.

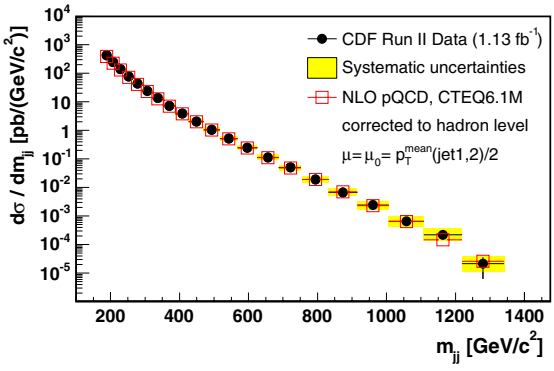

(a)

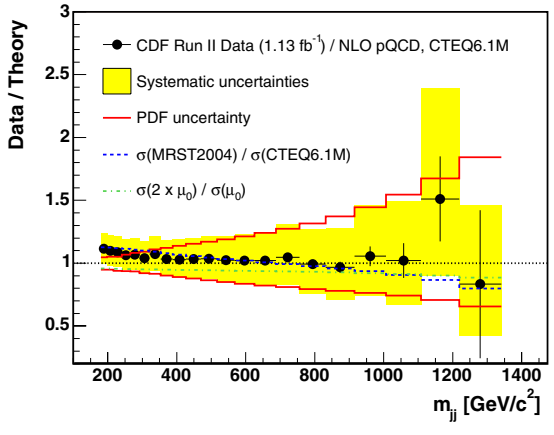

(b)

Fig. 14. (a) The measured dijet mass spectrum for both jets to have $|y| < 1$ compared to the NLO pQCD prediction obtained using the CTEQ6.1 PDFs. (b) The ratio of the data to the NLO pQCD prediction. The experimental systematic uncertainties, theoretical uncertainties from PDF, the ratio of MRST2004/CTEQ6.1, and the dependence on the choice of renormalization and factorization scales are also shown. An additional 6% uncertainty in the determination of the luminosity is not shown.

The D0 collaboration measured[31] normalized angular distributions in $\chi_{\text{dijet}} = \exp(|y_1 - y_2|)$. They are well-described by theory calculations at NLO in the strong coupling constant and are used to set limits on quark compositeness, ADD large extra dimensions,[32,33] and TeV^{-1} extra dimensions models.[34]

4. Photon Final States

4.1. *Inclusive photon production*

The high p_T photons emerge directly from $p\bar{p}$ collisions and provide a probe of the parton hard scattering process with a dominating contribution from qg initial state.

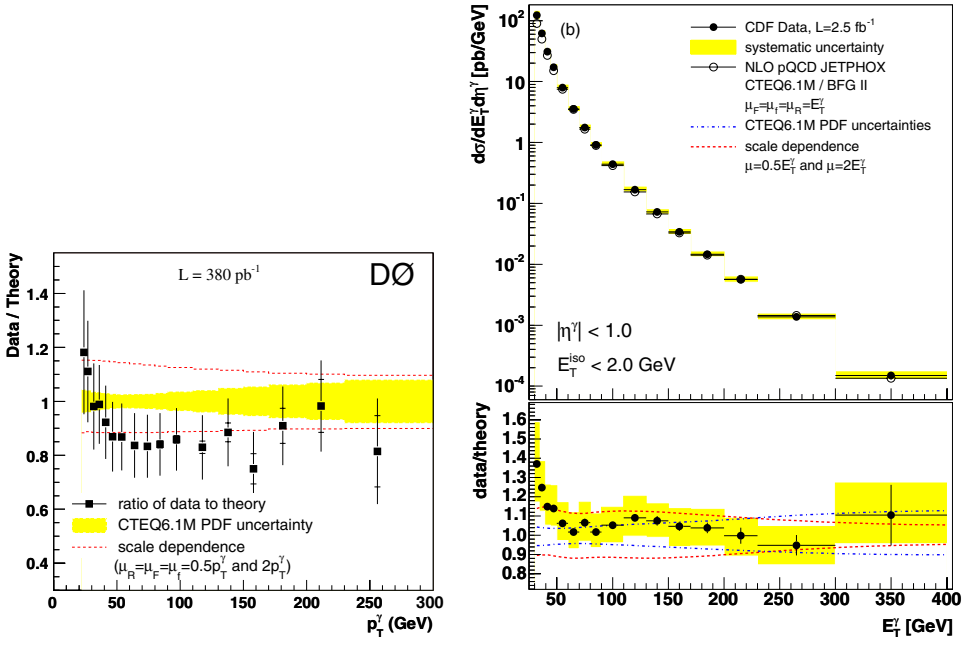

Fig. 15. The ratio of the measured cross-section to the theoretical predictions from JETPHOX. The plot (a) is for D0 and the plot (b) is for CDF measurements. The full vertical lines correspond to the overall uncertainty while the internal line indicates just the statistical uncertainty. Dashed lines represents the change in the cross-section when varying the theoretical scales by factors of two. The shaded region indicates the uncertainty in the cross-section estimated with CTEQ6.1M PDFs.

Being a direct probe of the parton dynamics, they are of a permanent interest in high energy physics. A few cross-section measurements were done in Run I (see Ref. 35). In Run II, the inclusive photon production cross-sections have been measured by D0 and CDF collaborations with photons in the central rapidity region.[36,37] The results shown in Fig. 15 are in agreement within experimental uncertainties between the two experiments, and both indicate some tension between NLO pQCD and data at low p_T.

The D0 and CDF inclusive photon data together with ATLAS and CMS data[38,39] have been used to constrain the gluon PDF at low x values.[40]

4.2. *Photon + jet production*

The production of a photon with associated jets in the final state is another powerful and direct probe of the dynamics of hard QCD interactions. As compared with the inclusive photon production, information about the accompanying jet allows to calculate parton fractions x in the leading order approximation (see e.g. Ref. 41). Different p_T^γ and angular configurations between the photon and the jets can be used to extend inclusive photon production measurements and simultaneously test

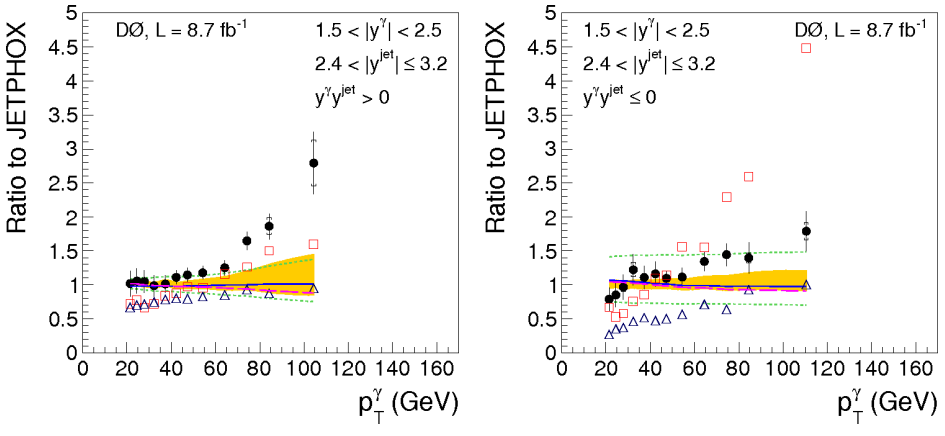

(a) (b)

Fig. 16. Ratios of the measured differential cross-sections of γ + jet production with forward photons and jet rapidity interval $2.4 < |y^{\rm jet}| \leq 3.2$ to the pQCD NLO prediction using JETPHOX[43] with the CT10 PDF set and $\mu_R = \mu_F = \mu_f = p_T^\gamma$. Plots (a) and (b) correspond to the same and opposite signs of photons and jet rapidities. The solid vertical line on the points shows the statistical and p_T-dependent systematic uncertainties added in quadrature, while the internal line shows the statistical uncertainty. The two dotted lines represent the effect of varying the theoretical scales of JETPHOX by a factor of two. The shaded region is the CT10[12] PDF uncertainty. The dashed and dash–dotted lines show ratios of the JETPHOX predictions with MSTW2008NLO[7] and NNPDFv2.1[10] to CT10 PDF sets. The predictions from SHERPA and PYTHIA are shown by the open squares and triangles, respectively.

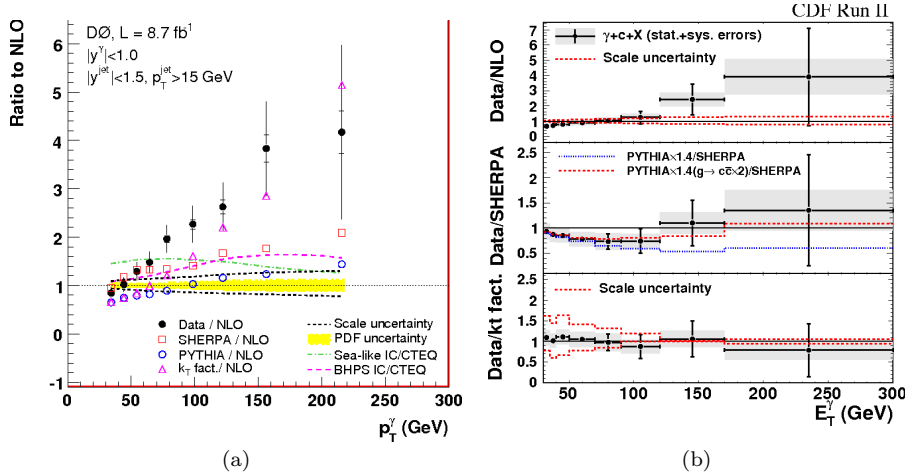

(a) (b)

Fig. 17. The ratio of measured $\gamma + c$-jet production cross-sections to predictions. The plot (a) is for D0 and the plot (b) is for CDF measurements. The uncertainties on the data include both statistical (inner error bar) and total uncertainties (full error bar). Also shown are the uncertainties on the theoretical QCD scales and the CTEQ6.6M PDFs. The ratio for intrinsic charm models[44] are presented. as well as the predictions given by $k_{\rm T}$-factorization,[50] SHERPA[15] and PYTHIA.[16] The result of increased $q\bar{q} \to \gamma + g(g \to c\bar{c})$ rates by a factor 1.4 in PYTHIA predictions is also shown (on the right).

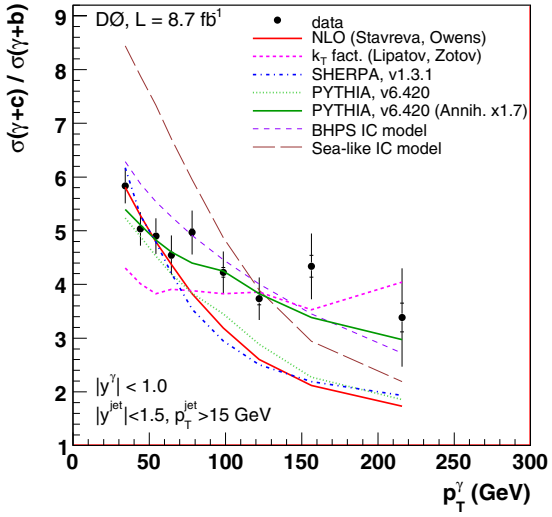

Fig. 18. The ratio of $\gamma + c$-jet and $\gamma + b$-jet production cross-sections for data together with theoretical predictions as a function of p_T^{γ}. The uncertainties on the data include both statistical (inner error bar) and total uncertainties (full error bar). Predictions given by k_{T}-factorization,[50] SHERPA[15] and PYTHIA[16] are also shown. The PYTHIA predictions with a contribution from the annihilation process increased by a factor of 1.7 are shown as well. The predictions for intrinsic charm models[44] are also presented.

the underlying dynamics of QCD hard-scattering subprocesses in different regions of x and hard-scattering scales Q^2.

The triple differential cross-section $\mathrm{d}^3\sigma/\mathrm{d}p_T^{\gamma}\mathrm{d}y^{\gamma}\mathrm{d}y^{\mathrm{jet}}$ for the associated inclusive photon and jet production process $p\bar{p} \to \gamma + \mathrm{jet} + X$ is measured for events with central ($|y^{\gamma}| < 1.0$) and forward ($1.5 < |y^{\gamma}| < 2.5$) photons in four jet rapidity intervals ($|y^{\mathrm{jet}}| \leq 0.8$, $0.8 < |y^{\mathrm{jet}}| \leq 1.6$, $1.6 < |y^{\mathrm{jet}}| \leq 2.4$, and $2.4 < |y^{\mathrm{jet}}| \leq 3.2$), for configurations with same and opposite signs of photon and jet rapidities.[42] The pQCD NLO predictions describe data with central photons in almost all jet rapidity regions except low p_T^{γ} ($< 40\,\mathrm{GeV}$) and the opposite-sign rapidity events at high p_T^{γ} with very forward jets ($2.4 < |y^{\mathrm{jet}}| < 3.2$), see Fig. 16. They also describe data with forward photons except for the same-sign rapidity events with $p_T^{\gamma} > 70\,\mathrm{GeV}$ and $2.4 < |y^{\mathrm{jet}}| \leq 3.2$. The measured cross-sections typically have similar or smaller uncertainties than the NLO PDF and scale uncertainties, and can be used as inputs to global fits determining gluon and other PDFs.

4.3. *Photon + heavy flavor jet production*

Study of events with photons produced in association with a $b(c)$-quark jet provides information about the $b(c)$-quark and gluon PDFs of the proton. At high p_T's, they are also sensitive to the events with double $b(c)$ quarks produced in the annihilation process $q\bar{q} \to \gamma g, g \to Q\bar{Q}$ ($Q = b, c$). These events also provide a test for the models with intrinsic charm and beauty.[44,45]

The D0 and CDF experiments have measured the differential cross-sections of $\gamma + b$-jet and $\gamma + c$-jet productions as a function of p_T^γ at the Fermilab Tevatron $p\bar{p}$ collider.[46–48] The results cover the kinematic range $30 < p_T^\gamma < 300\,\text{GeV}$, $|y^\gamma| < 1.0$, and $|y^{\text{jet}}| < 1.5$, see Fig. 17. In the same kinematic region, and in the same p_T^γ bins, D0 has also measured the $\sigma(\gamma+c)/\sigma(\gamma+b)$ cross-section ratio. None of the theoretical predictions considered (QCD NLO,[49] k_T factorization,[50] SHERPA and PYTHIA) give good description of the data in all p_T^γ bins, see Fig. 18. Such a description might be achieved by including higher-order corrections into the QCD predictions. At $p_T^\gamma \gtrsim 80\,\text{GeV}$, the observed difference from data may also be caused by an underestimated contribution from gluon splitting $g \to c\bar{c}$[51–53] in the annihilation process or by contribution from intrinsic charm.[44,45]

Production of $\gamma + 2$ b-jet events has been studied by D0 collaboration[54] differentially in p_T^γ bins. The ratio of differential production cross-sections for $\gamma + 2$ b-jet to $\gamma + b$-jet is also measured, see Fig. 19. The ratio agrees with the predictions from NLO QCD and k_T-factorization approach within the theoretical and experimental uncertainties in the full studied p_T^γ range while is not described by SHERPA and PYTHIA generators.

4.4. *Diphoton production*

In light of the Higgs boson search and other possible resonances decaying to a photon pair, both collaborations performed a thorough study of diphoton production.

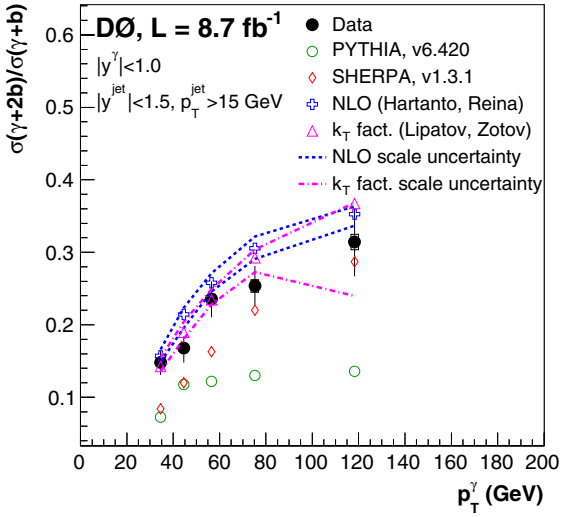

Fig. 19. The ratio of $\gamma + 2$ b-jet to $\gamma + b$-jet production cross-sections for data together with theoretical predictions as a function of p_T^γ. The uncertainties on the data points include both statistical (inner error bar) and the full uncertainties (full error bar). The measurements are compared to the NLO QCD calculations.[55] The predictions from SHERPA,[15] PYTHIA[16] and k_T-factorization[50] are also shown along with the scale uncertainties on NLO and k_T-factorization prediction.

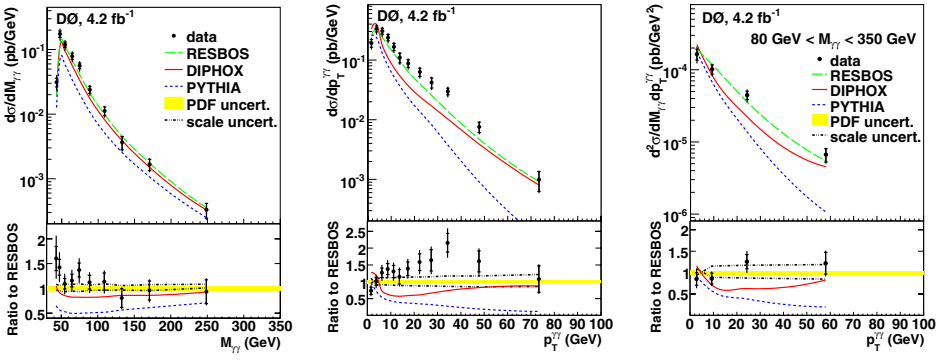

(a) (b) (c)

Fig. 20. The measured double differential diphoton production cross-sections as functions of $M_{\gamma\gamma}$ (a), $q_T^{\gamma\gamma}$ for $30 < M_{\gamma\gamma} < 50\,\text{GeV}$ (b), and $M_{\gamma\gamma} > 80\,\text{GeV}$ (c) by the D0 experiment.

D0 measured the diphoton cross-sections as a function of the diphoton mass $M_{\gamma\gamma}$, the transverse momentum of the diphoton system $q_T^{\gamma\gamma}$, the azimuthal angle between the photons $\Delta\phi_{\gamma\gamma}$, and the polar scattering angle of the photons. The latter three cross-sections are measured in the three $M_{\gamma\gamma}$ bins, 30–50, 50–80 and 80–350 GeV. The photons are considered with $|\eta| < 0.9$, $p_{T,1} > 21$, $p_{T,2} > 20\,\text{GeV}$ and also requiring $q_T^{\gamma\gamma} < M_{\gamma\gamma}$ to reduce the contribution from the fragmentation photons.[56] The measurements are compared to NLO QCD (provided by RESBOS[56] and DIPHOX[57]) and PYTHIA[16] predictions, see Fig. 20. The results show that the largest discrepancies between data and NLO predictions for each of the kinematic variables originate from the lowest $M_{\gamma\gamma}$ region ($M_{\gamma\gamma} < 50\,\text{GeV}$), where the contribution from $gg \to \gamma\gamma$ is expected to be largest.[58] The discrepancies between data and the theory predictions are reduced in the intermediate $M_{\gamma\gamma}$ region, and a quite satisfactory description of all kinematic variables is achieved for the $M_{\gamma\gamma} > 80\,\text{GeV}$ region, the relevant region for the Higgs boson and new phenomena searches. The CDF collaboration

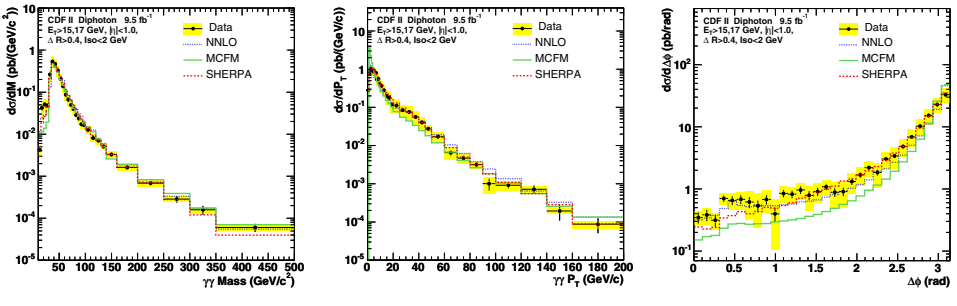

(a) (b) (c)

Fig. 21. The measured differential diphoton production cross-sections as functions of $M_{\gamma\gamma}$ (a), $q_T^{\gamma\gamma}$ (b) and $\Delta\phi_{\gamma\gamma}$ (c) by the CDF experiment.

has also measured the diphoton production cross-sections functions of $M_{\gamma\gamma}$, $q_T^{\gamma\gamma}$ and $\Delta\phi_{\gamma\gamma}$.[59] They are shown in Fig. 21. None of the models describe the data well in all kinematic regions, in particular at low diphoton mass ($M_{\gamma\gamma} < 60\,\text{GeV}$), low $\Delta\phi_{\gamma\gamma}(< 1.7$ rad) and moderate $q_T^{\gamma\gamma}$(20–50 GeV). Both experiments have also studied the diphoton production in separate kinematic regions, with $\Delta\phi_{\gamma\gamma} < \pi/2$ and $\Delta\phi_{\gamma\gamma} > \pi/2$, as well as for different $q_T^{\gamma\gamma}$selections.[60,61]

Measurements of the diphoton cross-section done by CMS[62] and ATLAS[63] experiments provide a complementary information to the extensive studies done by D0 and CDF experiments.

5. W/Z + Jets Final States

5.1. W/Z + jet *production*

The production of W or Z with accompanying hadronic jets provides quantitative tests of QCD through comparison of the rate of multijet production as a function of the strong coupling constant and comparison of various kinematic distributions with the theoretical predictions to probe the underlying matrix elements. In addition, events with multiple jets in association with W or Z form a background for a variety of physics processes, including Higgs boson, top quark production and supersymmetry searches.

In Run I study of W and Z boson production in association with jets were initiated by measurement of ratio of $W+1$ jet to $W+0$ jet events,[68] the measurement of the cross-section and study of kinematic properties of direct single W boson production with jets,[64] study of jet properties in Z + jets[65,66] and study of color coherence effects in W + jet events.[67]

Large data sample in Run II allowed both CDF and D0 experiments to conduct extensive studies of W and Z boson production in association with jets.

The D0 collaboration published a comprehensive analysis of inclusive $W(\to e\nu)$ + n-jet production for $n \geq 1, 2, 3, 4$ using $3.7\,\text{fb}^{-1}$ of data.[69] Differential cross-sections are presented as a function of many observables, such as jet rapidities, lepton transverse momentum, leading dijet p_T and invariant mass, etc. Many of the variables were studied for the first time in W + n-jet events, e.g. a probability of the third jet emission as a function of dijet rapidity separation in inclusive W + 2-jet events (such a variable is important for understanding the Higgs boson via vector-boson fusion, and also sensitive to BFKL-like dynamics). The data corrected for detector effects and the presence of backgrounds is compared to a variety of theoretical predictions. Figure 22 shows the differential distributions of W + n-jet events as functions of H_T, the scalar sum of the transverse energies of the W boson and all $p_T > 20\,\text{GeV}$ jets in the event. This variable is often used as the renormalization and factorizations scale for theoretical predictions for vector boson plus jets processes, so accurate predictions of H_T are important. There is significant variation in the shapes of the H_T spectrum from the various theoretical predictions, PYTHIA, SHERPA, HERWIG, ALPGEN show discrepancies of

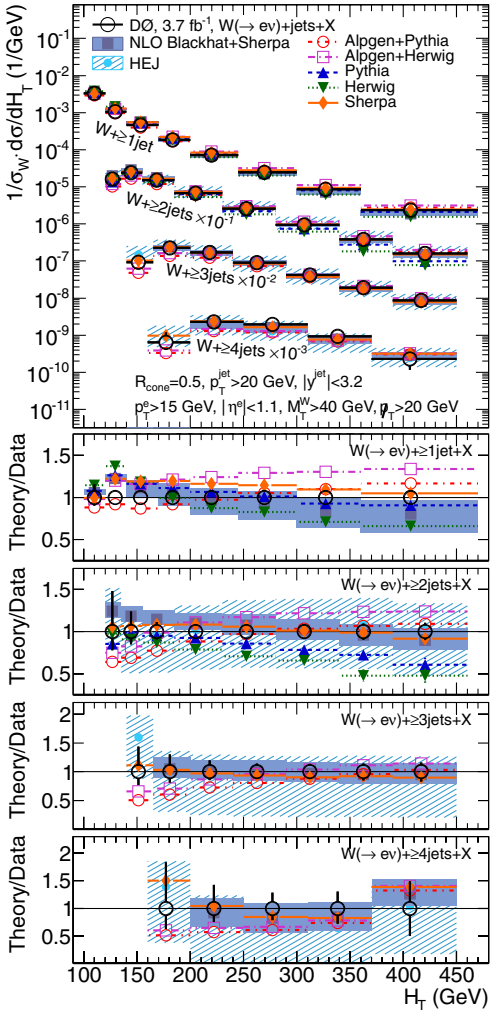

Fig. 22. Measurement of the distribution of the scalar sum of transverse energies if the W boson and all jets and comparison to various theoretical predictions. Lower panels show theory/data comparisons for each of the n-jet multiplicity bin results separately.

the order of 25% in one-jet bin and up to 50% in 4-jet bin. This data is significantly more precise than theoretical predictions and can be used to improve the modeling.

The CDF experiment presented similarly extensive analysis of $Z/\gamma^\star(\to +e^+e^-, \mu^+\mu^-) +$ jets production utilizing the full CDF dataset of $9.6\,\mathrm{fb}^{-1}$.[70] The cross-sections are unfolded to the particle level and combined. Results for various observables are compared with the most recent theoretical predictions. In addition, the effect of NLO electroweak virtual corrections[72] on the $Z\gamma^\star +$ jet production has been studied and included in the comparison with the measured cross-section.

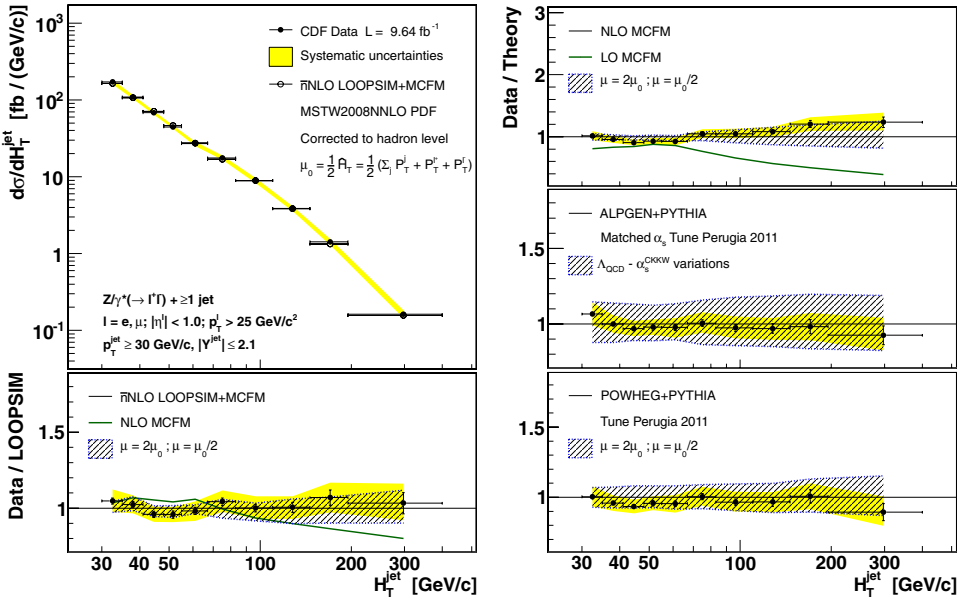

Fig. 23. (Color online) Measurement of the $Z/\gamma^{\star}+\geq 1$ jet differential cross-section as a function of $H_T^{\rm jet} = \Sigma p_T^{\rm jet}$. The lower and right panels show the data/theory ratio with respect to the theoretical predictions, with blue bands showing the scale uncertainty of each prediction, and yellow band corresponding to the experimental systematic uncertainty.

Figure 23 shows measurement of the differential cross-section as a function of $H_T^{\rm jet} = \Sigma p_T^{\rm jet}$ variable similar to one described previously. The approximate NNLO LOOPSIM + MCFM ($\bar{n}$NLO) prediction[71] used with NNLO PDF and 3-loop running α_S provides better modeling of the data distribution and shows a significantly reduced scale uncertainty.

5.2. W/Z + heavy *flavor jet production*

The measurement of the W boson production in association with a b-quark jet provides an important test of QCD, as it is sensitive to heavy-flavor quarks in the initial state. $W + b$-jet production is a large background to searches for the Higgs boson in WH production with a decay of $H \to bb$, to measurements of top quark properties in single and pair production, and to searches for physics beyond the Standard Model. The CDF collaboration published results for the cross-section for jets from b quarks produced with W boson using 1.9 fb^{-1} of data.[73] The events were selected by identifying electron or muon decays of W and containing one or two jets with $E_T > 20$ GeV and $|\eta| < 2.0$. The measured b-jet production cross-section of $\sigma \times B(W \to \ell\nu) = 2.74 \pm 0.27(\text{stat}) \pm 0.42(\text{syst})$ pb is higher than theoretical predictions based on NLO calculations of $1.22 \pm 0.14(\text{syst})$ pb.

The D0 collaboration published results for the same process based on a data sample of 6.1 fb^{-1}.[74] The combined results for electron and muon channels, defined

using a common phase space for $p_T^{e,\mu} > 20\,\text{GeV}$, $|\eta^\mu| < 1.7$ ($|\eta^e| < 1.1$ or $1.5 < |\eta^e| < 2.5$), $p_T^\nu > 25\,\text{GeV}$, $p_T^{\text{b-jet}} > 20\,\text{GeV}$, $|\eta^{\text{b-jet}}| < 1.1$, are $\sigma(W \to \ell\nu) + b + X) = 1.05 \pm 0.12(\text{stat} + \text{syst})$ pb for $|\eta^\ell| < 1.7$. The result is in agreement with NLO predictions using MCFM v6.1[75] based on CTEQ6M PDF[8] $1.34^{+0.41}_{-0.34}$ pb as well as with predictions from the SHERPA and MADGRAPH[76] Monte Carlo event generators.

The study of associated production of a W boson and a charm quark at hadron colliders provides direct access to the strange-quark content of the proton at an energy scale of the order of the W-boson mass. This sensitivity is due to the dominance of strange quark–gluon fusion. At leading order the production of W boson with single charm in $p\bar{p}$ collisions is described by the scattering of a gluon with a d, s or b quark; however at the Tevatron the large d quark PDF in the proton is compensated by the small quark-mixing CKM matrix element $|V_{cd}|$, while contribution from $gb \to Wc$ is heavily suppressed by $|V_{cb}|$ and b quark PDF. The CDF collaboration presented the first observation of the production of W boson with a single charm quark jet in $p\bar{p}$ collisions at $\sqrt{s} = 1.96\,\text{TeV}$.[77] The charm quark is identified through the semileptonic decay of the charm hadron into an electron or muon, *soft lepton*, so charm jets are required to have an electron or muon candidate within the jet, so-called *soft lepton tagging*, while the W boson is identified through its leptonic decay by looking for an isolated electron or muon carrying large transverse energy E_T and large missing $\not\!\!E_T$ in the event. Events are classified based on whether the charge of the lepton from W boson and the charge of the soft lepton are of opposite signs or the same sign. The Wc signal is observed with a significance of 5.7 standard deviations. The production cross-section for $p_{T_c} > 20\,\text{GeV}$ and $|\eta_c| < 1.5$ is $\sigma_{Wc} \times B(W \to \ell\nu) = 13.5^{+3.4}_{-3.1}$ pb and is in agreement with theoretical predictions.

Measurements of the production for a Z boson in association with b jets were published by the CDF and D0 collaborations. Both results provide good agreement with the theoretical predictions. The D0 experiment utilized $4.2\,\text{fb}^{-1}$[79] of data for $Z \to +\ell\ell$ events with a jet with $p_T > 20\,\text{GeV}$ and pseudorapidity of $|\eta| \leq 2.5$ to measure the ratio of Z + b-jet to Z + jet cross-sections of 0.0193 ± 0.0027. The CDF results[78] correspond to the ratio of integrated $Z + b$ jet cross-sections to the inclusive Z production for jets with $E_T \geq 20\,\text{GeV}$ and $|\eta| < 1.5$ and is $3.32 \pm 0.53(\text{stat}) \pm 0.42(\text{syst}) \times 10^{-3}$. The predictions from Monte Carlo generators and NLO QCD calculations are consistent with this result.

The D0 collaboration extended the study of $Z + b$-jet production by utilizing the full D0 data set of $9.7\,\text{fb}^{-1}$.[80] The ratios of the differential cross-sections as a function of p_T^Z (a) and p_T^{jet} (b) are presented in Fig. 24 compared with MCFM, ALPGEN, SHERPA predictions. None of the predictions used provide a consistent description of the variables.

The D0 collaboration reported the first measurement of associated charm jet production with a Z boson.[81] Results are presented as measurements of the ratio of cross-sections for the $Z + c$ jet to Z + jet production as well as the $Z + c$ jet to $Z + b$ jet production in events with at least one jet to benefit from the cancellation

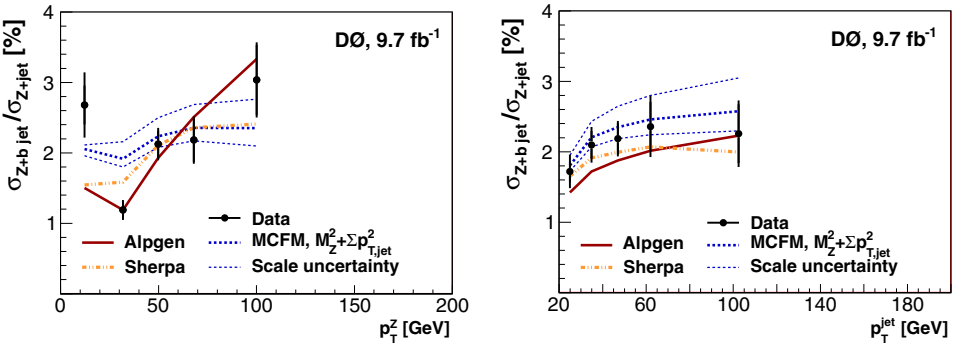

(a) (b)

Fig. 24. Ratio of the differential cross-section for p_T^Z (a) and $p_T^{\rm jet}$ (b). The error bars include statistical and systematic uncertainties added in quadrature. the scale uncertainty band represent the variation of the renormalization and factorization scales by a factor of 2.

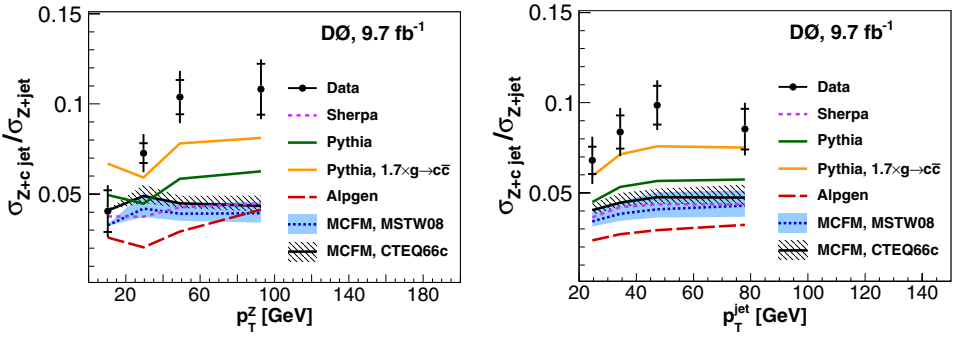

(a) (b)

Fig. 25. Ratios of the differential cross-sections of $Z+c$-jet to $Z+$jet as a function of (a) p_T^Z and (b) $p_T^{\rm jet}$. The uncertainties if the data include statistical (inner error bars) and full uncertainties (entire error bars).

of some systematic uncertainties. This analysis is based on the complete Run II D0 data set of 9.7 fb^{-1}. The ratios of differential cross-sections as a function of $p_T^{\rm jet}$ and p_T^Z are compared to various predictions in Fig. 25. On average, the NLO predictions significantly underestimate the data. Perugia-0 tune with CTEQ6L1 PDF set are used for PYTHIA comparison. Improvement in predictions can be achieved by enhancing the default rate of $g \to c\bar{c}$ in PYTHIA by a factor of 1.7, motivated by the $\gamma + c$ jet production measurements at the Tevatron discussed in Sec. 4.3.

6. Soft QCD

The theory of strong interactions, QCD, is very successful in describing processes where a hard scale is present, either given by a large transverse momentum, p_T, or

by a large mass of the exchanged particles, or a highly virtual particle. In these types of processes the strong coupling constant, α_S, is small enough to allow for perturbative calculations to be valid. Soft interactions, which are usually understood as the interactions of hadrons at a relatively small scale, or low p_T, although making up the bulk of the hadronic cross-section, lack precise theoretical predictions in the absence of the hard energy scale needed for the perturbative QCD calculations to converge. The fundamental importance to improve our understanding of soft strong interactions can be demonstrated by the lack of reliable predictions for such important quantities as the total hadronic cross-section, cross-sections for elastic scattering of hadrons, or the mass and size of the proton. From the practical point of view, the majority of collisions produced at the colliders belong to the category of "soft processes" and thus are very important to the modeling of the background activity.

Hadron–hadron collisions can be divided into several categories. Elastic scattering is a 2-to-2 color singlet exchange process in which two outgoing particles are the same as the two incoming particles. This process is described by the single variable t, squared four-momentum transfer. Single (double-) diffraction corresponds to the color singlet exchange between the initial hadrons, where for single (double) diffraction one (both) of the incoming particles is (are) excited into a high mass color singlet state, with the mass M_X (M_X and M_Y), which then decays. This process can be described in terms of the variables, t, and either mass M_X (M_X and M_Y), or the fractional energy loss of the intact proton (and antiproton) $\xi = M_X^2/s$ ($\xi_1 = M_X^2/s$ and $\xi_2 = M_Y^2/s$). The nondiffractive production includes all processes not described by the elastic and diffractive channels. In this case, particle production is taking place through all available rapidity space.

6.1. *Nondiffractive production*

6.1.1. *Minimum bias studies*

The minimum bias final state observables represent a complicated mix of different physics effects ranging from purely soft to very "hard" ones. The term *minimum bias* is a generic term which refers to events that are selected with very minimal trigger, to ensure that they are as inclusive as possible, and so as a result the definition of minimum bias differs from experiment to experiment. The majority of minimum bias events are "soft" and thus processes under these conditions are notoriously difficult to model. While the understanding of softer physics is interesting in its own right, a detailed understanding of minimum bias interactions is extremely important in very high luminosity environments where a large number of such interactions happen in the same bunch crossing. At the CDF experiment studies of minimum bias events were initiated at Run I when inclusive charged particle distributions at $\sqrt{s} = 1800\,\text{GeV}$ were measured,[83] as well as studies of different variables, such as the multiplicity, transverse momentum p_T, average p_T for soft and hard interactions at $\sqrt{s}$ of 630 GeV and 1800 GeV were performed. At Run II the CDF collaboration continued minimum bias studies by providing first measurement[84] of the

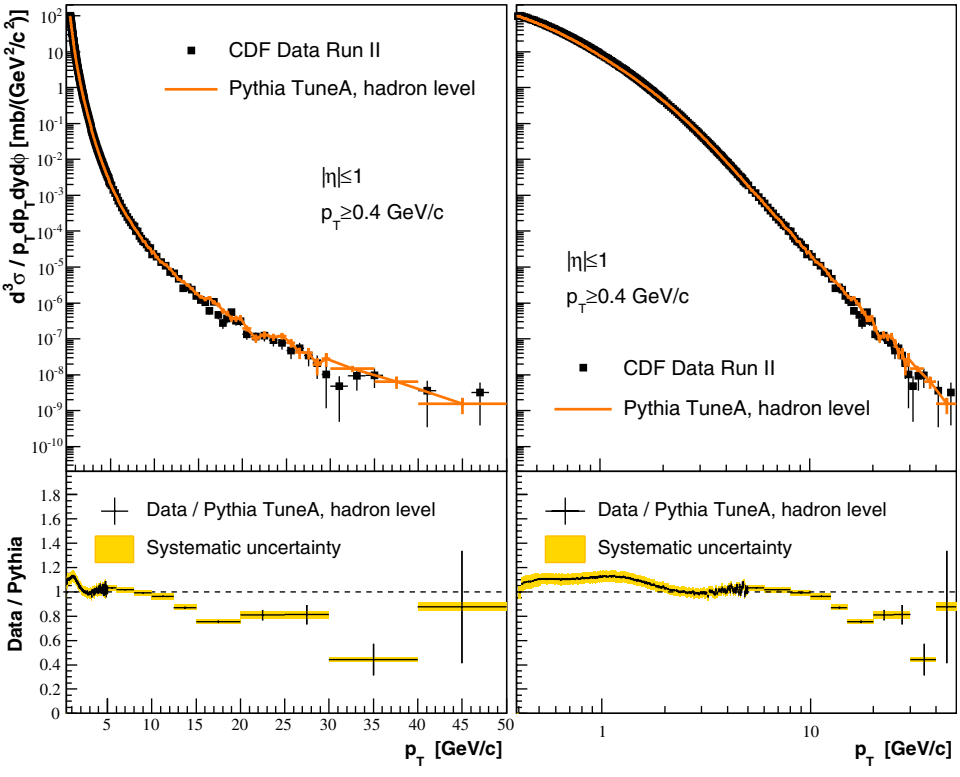

Fig. 26. Comparison of the track p_T differential cross-section with PYTHIA Tune A prediction at hadron level. The data error bars describe the statistical uncertainty on the data and the statistical uncertainty on the total correction.

event transverse energy sum differential cross-section representing an attempt at describing the full final state including neutral particles, by studying particle transverse momentum as a function of the event particle multiplicity, and significantly extending the range of the inclusive charged particle transverse momentum differential cross-section while improving precision. The analysis was based on 506 pb^{-1} data sample collected with CDF minimum bias trigger implemented by means of two sets of Cherenkov counters placed on both sides of the detector and requiring a coincidence of both signals. The resulting MB sample contains most of the inelastic cross-section with a small contamination of single- and double-diffractive. Figure 26 shows a comparison of track p_T differential cross-section with PYTHIA Tune A prediction at hadron level. Data and Monte Carlo prediction show good agreement.

6.1.2. *Underlying event studies*

The existence of Monte Carlo models that accurately simulate QCD hard-scattering events is essential for all *new* physics searches at hadron–hadron colliders. To achieve a given accuracy one should be able to have not only a good model of the hard

scattering part of the process, but also of the *underlying event* corresponding to all final state particles produced beyond those associated with the hardest scattering, an unavoidable background to most collider observables. The sources of the underlying event are beam–beam remnants (BBR) and activity from multiple parton interactions (MPI). The CDF pioneered a method providing a comprehensive set of measurements subjecting to the rigorous scrutiny particle production associated with the underlying event in a model-independent way. Run II studies of the underlying event were extended to the comparison of Drell–Yan production and leading jet topologies.[86] For Drell–Yan production, the final state includes a lepton–antilepton pair, and there is no colored final state radiation, thus providing a clean way to study the underlying event (UE). The methodology of the presented study is similar to previous CDF UE studies,[85] by considering the *toward*, *away*, and *transverse* regions defined by the azimuthal angle $\Delta\phi$ relative to the direction of the leading jet in the event, or the direction of the lepton-pair in Drell–Yan production ($\Delta\phi = \phi - \phi_{\mathrm{jet}_1/\mathrm{pair}}$), see Fig. 27(a). We study charged particles with $p_T > 0.5\,\mathrm{GeV}$ and $|\eta| < 1$ in the above-mentioned regions. For high-p_T jet production the leading jet in the event, reconstructed with the Midpoint algorithm, and with $|\eta_{\mathrm{jet}}| < 2$ was required. For Drell–Yan production the requirement of the invariant mass of the lepton-pair to be in the mass region of the Z-boson, $70 < M_{\mathrm{pair}} < 110\,\mathrm{GeV}$, with $|\eta_{\mathrm{pair}}| < 6$ was placed. For leading jet events, the toward and away regions are characterized by large contributions from the outgoing high energy jets, whereas the transverse region is perpendicular to the plane of the hard scattering and is sensitive to the underlying event. For Drell–Yan events, while the away region receives large contributions from the balancing jet, both the toward and transverse regions are sensitive to the underlying event. Many observables were studied for all three regions of interest. Here, we will describe just one, the charged particle density, $dN/d\eta d\phi$ in the transverse region for both the leading jet and Drell–Yan topologies, see Fig. 27(b). The underlying event observable is found to be reasonably flat with the increasing lepton pair transverse momentum and quite similar for both

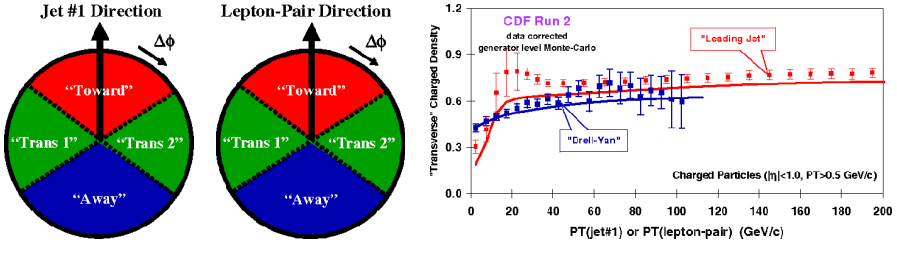

(a) (b)

Fig. 27. (a) Schematic division of different regions in azimuthal angle $\Delta\phi$ relative to the direction of the leading jet in the event or the direction of the lepton pair in Drell–Yan production; (b) the density of charged particles in the transverse region for leading jet and Drell–Yan events compared with PYTHIA Tune A and PYTHIA Tune AW.

topologies. The small "bump" for low-p_T values for leading jet distribution reflects the fact that there are many low p_T jets and for this $p_T < 30\,\text{GeV}$ values the leading jet is not always the jet resulting from the hard two-to-two scattering. PYTHIA Tune A for leading jet events, and PYTHIA Tune AW for Drell–Yan events provide reasonable agreement with the experimental data.

6.1.3. *Particle production*

The measurements of the production of particles with different quark flavors and number of quarks is an essential step in understanding hadron production. Since the strange quark is heavier than the up and down quarks, strange hadron production is usually suppressed, with an amount of suppression used for refining the phenomenological models and parameters of the Monte Carlo models. At the same time, the enhanced production of the strange particle has been frequently suggested as a manifestation of the formation of quark–gluon plasma. The CDF collaboration presented measurements of Λ^0, $\bar{\Lambda}^0$, $\Xi^{\pm}$, and $\Omega^{\pm}$ hyperons under minimum bias conditions[87] and K^0_S, $K^{\star\pm}(892)$ and ϕ^0 in minimum bias events and K^0_S and Λ^0 in jets.[88] All particles were reconstructed in the central region with $|\eta| < 1.0$, and for minimum bias produced particles with p_T up to 10 GeV and particles in jets with p_T up to 20 GeV. From the ratio of cross-sections, see Fig. 28(b), it is clear that cross-sections depend on the number of strange quarks, however very similar p_T slopes for distributions on Fig. 28(a) indicate a universality in particle production as p_T increases. Results of Ref. 88 also demonstrate that the ratio of Λ^0 to K^0_S as a function of p_T in minimum bias events becomes similar to the fairly constant ratio in jets at $p_T \sim 5\,\text{GeV}$. This confirms the earlier observation from CDF underlying event studies that particles with $p_T \geq 5\,\text{GeV}$ in minimum bias events are from "soft" jets and that the p_T slope of particles in jets is insensitive to light

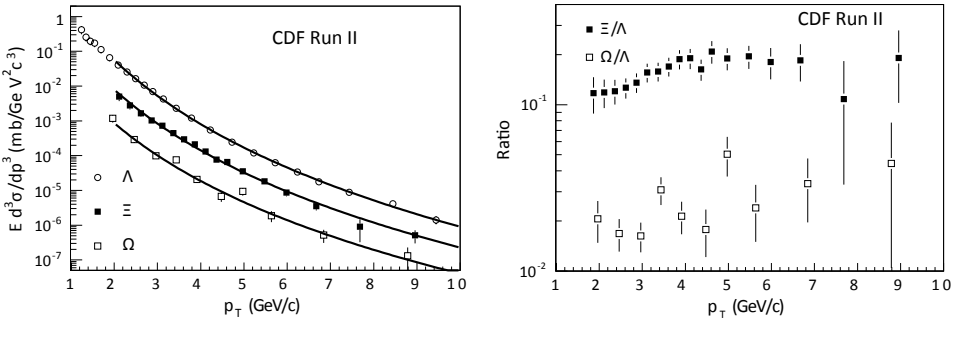

Fig. 28. The inclusive invariant p_T differential cross-section distributions for Λ^0, Ξ^- and Ω^- for $|\eta| < 1$ uncertainties for data points include all statistical and systematic uncertainties except one associated with normalization uncertainty due to the minimum bias trigger cross-section. The solid curves are from fits to a power law function; (b) the ratios of Ξ^-/Λ^0 and Ω^-/Λ^0 as a function of p_T.

quark flavor and to the number of valence quarks. These results are providing an important contribution for tuning of Monte Carlo models.

6.1.4. *Fragmentation studies*

The transition from partons to hadrons, or *hadronization*, is not understood from perturbative QCD and has to be described by a phenomenological model. Detailed studies of jet fragmentation allow us to understand the relative roles of the perturbative and nonperturbative stages of jet formation and to probe boundaries of parton shower and hadronization. The characteristics of soft particle production, such as particle multiplicities, inclusive distributions and correlation functions can be described by analytical predictions of the next-to-leading log approximation (NLLA)[89] describing parton shower formation supplemented with the local parton–hadron duality approach[90] prescribing that hadronization process takes place locally and thus applies perturbative predictions at the partonic level directly to hadronic distributions. Past studies of inclusive particle distributions at e^+e^- experiments[92] and CDF[93] have given strong support to this theoretical framework. In Run II the CDF collaboration extended studies to the measurements of the two-particle momentum correlations in jets as a function of jet energy.[94] The correlation function is introduced as $\xi = \ln E_{\text{jet}}/p_{\text{hadron}}$ and is defined as a ration of two- and on-particle inclusive momentum distributions: $C(\Delta\xi_1, \Delta\xi_2) = D(\xi_1, \xi_2)/(D(\xi_1)D(\xi_2))$, where both inclusive distributions $D(\xi) = \ln(d\eta/d\xi)$ and $D(\xi_1, \xi_2)$ are normalized to unity. The results are obtained for charged particle within a restricted cone with an opening angle of $\theta_c = 0.5$ radians around the jet axis for events with dijet masses between 66 GeV and 563 GeV with underlying event contributions subtracted using the complimentary cones technique. The characteristic features of the theoretical predictions are follows: the correlation should be stronger for partons with equal momenta, or $\Delta\xi_1 = \Delta\xi_2$, and the strength of this effect should increase for lower momentum partons. Figure 29 shows overall good agreement between the data and theoretical predictions based on Fong–Webber calculation[82] that provided the predictions at the level of NLLA precisions, the modified leading log approximation (MLLA)[95] referred in Fig. 29 as Ramos approach, is an approach similar to NLLA but including higher-order terms ($\alpha_S^n \ln^{2n-2} E_{\text{jet}}$ and higher). The data follows the theoretical trends and shows an enhanced probability of finding two particles with the same value of momenta, indicated by the parabolic shape of the $\Delta\xi_1 = -\Delta\xi_2$ central diagonal profile with maximum at $\Delta\xi_1 = \Delta\xi_2 = 0$, with the effect becoming larger for particles with lower momenta, represented by the positive slope of the $\Delta\xi_1 = \Delta\xi_2$ central diagonal profile.

The measurement of the transverse momenta of particles in jets with respect to the jet axis, k_T[96] allows probing for softer particle spectra than from the previously discussed observables. The CDF measurement is based on $1\,\text{fb}^{-1}$ of data in events with dijet masses between 66 GeV and 737 GeV. The shape of k_T distribution is compared to the theoretical predictions from MLLA and NMLLA, next-to-leading

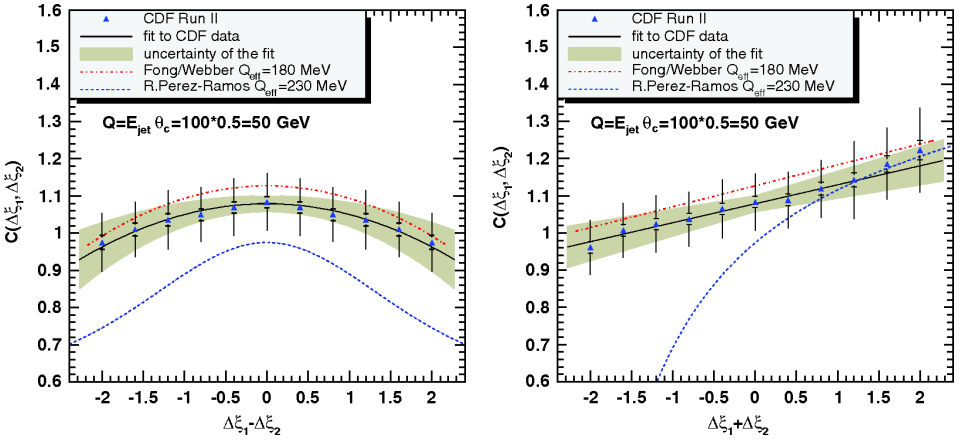

(a) (b)

Fig. 29. Central diagonal profiles $\Delta\xi_1 = -\Delta\xi_2$ (a) and $\Delta\xi_1 = \Delta\xi_2$ (b) of two-particle momentum correlations in jets in the restricted cone of size $\theta_c = 0.5$ radians for dijet mass bin with $Q = 50\,\text{GeV}$. The correlation in data is compared to that of theory.

log approximation,[97] as well as for PYTHIA Tune A Monte Carlo generator. The NMLLA results for $Q_{\text{eff}} = 230\,\text{MeV}$ provide an excellent description of the data over the entire range of particle k_T and dijet masses used in this measurement. Predictions of Monte Carlo generators for final stable particles are in agreement with the results obtained from data. The good qualitative agreement between NMLLA predictions and charged hadrons from PYTHIA Tune A is due to the tunings of the hadronization parameters in PYTHIA Tune A, discussed previously, while distribution from PYTHIA at the parton level shows significant deviations.

6.1.5. *Event shapes*

Event shapes describe geometric properties of the energy flow in the QCD final states by encoding information about the energy flow of an event in a continuous fashion. By having sensitivity to both perturbative and nonperturbative aspects of QCD they can be an important addition to the jet fragmentation studies. Event shapes have been studied extensively in e^+e^- and DIS experiments.[91] However, at hadron colliders they have received far less attention, primarily due to the difficulties in the theoretical description associated with the environment. From a theoretical point of view, a description over the full range of an event shape observable at a hadron collider requires not only perturbative QCD calculations but also the inclusion of a phenomenological model of the underlying event. The CDF collaboration performed studies[98] of transverse thrust and thrust minor, both defined in the plane perpendicular to the beam direction to reduce the conflict between requirements of calculations for variables to be "global" and reality of the limited detector coverage of any collider experiment. By using energies from unclustered calorimeter towers

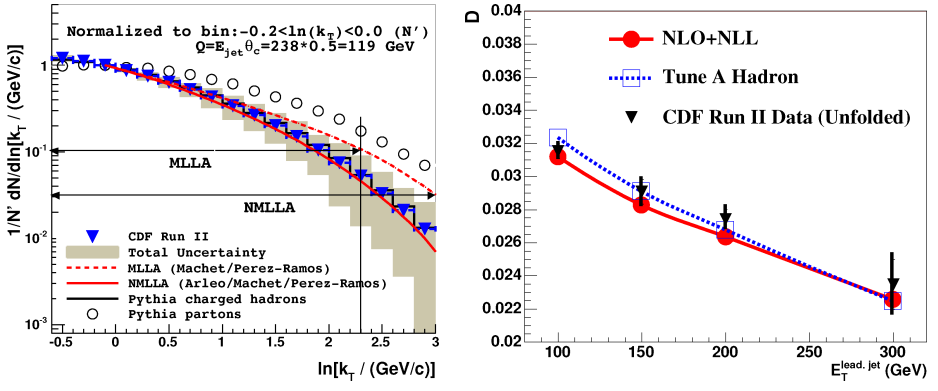

(a) (b)

Fig. 30. (a) Measured k_T distribution of particles in the restricted cone of size $\theta_c = 0.5$ around the jet axis in dijet mass bin of $Q = 119\,\text{GeV}$. The data are compared to the analytical predictions MLLA and NMLLA and to the predictions of the PYTHIA Tune A for partons and charged hadrons. Ranges of validity for MLLA and NMLLA predictions are shown by arrows; (b) the CDF corrected results for the dependence of the thrust differential on the transverse energy of the leading jet. The experimental results are compared with a parton-level NLO + NLL calculation and with PYTHIA Tune A at the hadron level. The error bars correspond to statistical and systematic uncertainties added in quadrature.

to measure the variables one can be free from the arbitrariness associated with jet definition. The transverse-thrust variable τ is defined to vanish in the limit of two back-to-back objects, and for the isotropic event $\tau = 1 - 2/\pi$, while the transverse-thrust minor T_{min} is a measure of the out-of-plane transverse momentum and varies from zero for an event in the event plane to $2/\pi$ for a cylindrically symmetric event. Both τ and T_{min} are sensitive to the modeling of the underlying event and agree with the distributions obtained from the PYTHIA Tune A. These observables can be used to improve the modeling of the underlying event. In addition to these variables, a new variable, *thrust differential*, constructed to be less sensitive to the underlying event and hadronization effects, was introduced by taking the weighted difference of the mean values of the thrust and thrust minor over the event sample. The evolution of this quantity as a function of the leading jet energies allows to have meaningful comparison between data and the theoretical predictions. As can be seen from Fig. 30(b), both the PYTHIA Tune A and resummed next-to-leading-logarithm (NLL) parton-level predictions that were matched to fixed-order results at next-to-leading-order (NLO), referred to as NLO + NLL calculations,[99] describe the data quite well. This study illustrates the need to include underlying event contributions when comparing data with pQCD in hadron–hadron collisions.

6.2. *Elastic scattering*

Elastic scattering $p\bar{p} \to p\bar{p}$ is a very important process that probes the structure of the proton. It is characterized by different t-dependencies, starting with the

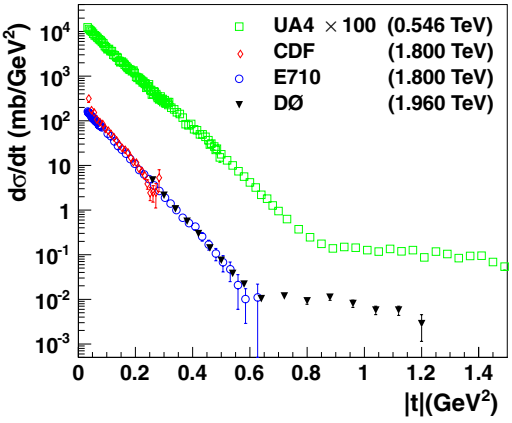

Fig. 31. The $d\sigma/dt$ cross-section as a function of t compared to the results from the CDF, E710 and the UA4 experiments.

lowest values of t: the Coulomb region where elastic scattering is dominated by photon exchange, the nuclear/Coulomb interference region; the "single pomeron exchange region", where $d\sigma/dt$ is proportional to e^{-bt}, followed by a region with a local diffractive minimum which moves to lower $|t|$ values as $\sqrt{s}$ increases, so-called *shrinkage*, and a high $|t|$ region described by perturbative QCD.

The D0 collaboration extended the $|t|$ range previously measured by CDF ($0.025 < |t| < 0.29\,\text{GeV}$)[100] to $0.26 < |t| < 1.2\,\text{GeV}$.[101] The elastically scattered protons and antiprotons were tagged with the forward proton detector spectrometer system. The data sample corresponds to an integrated luminosity of $31\,\text{nb}^{-1}$ and was collected with dedicated beam conditions. Figure 31 shows the measured $d\sigma/dt$ differential cross-section. The uncertainties correspond to the total experimental systematic uncertainties not including the 14% normalization uncertainty. The distribution shows a change in the $|t|$ dependence. The fit to the $d\sigma/dt$ in the region of $|t|$ from 0.25–0.6 GeV ^{2} with an exponential function $Ae^{-b|t|}$ provides a logarithmic slope parameter $b = 16.86 \pm 0.10(\text{stat}) \pm 0.20(\text{syst})$ in agreement with previous measurements from the CDF and E710 experiments.[102] Comparison in shape to data from UA4 collected at the $\sqrt{s} = 546\,\text{GeV}$[103] confirms the presence of the *shrinkage* as diffractive minima move toward lower $|t|$ values.

6.3. *Diffractive processes*

Diffractive reactions, which constitute a substantial fraction of the total cross-section in hadron–hadron scattering, can be described in terms of the *pomeron* ($I\!P$) exchange, a hypothetical object with the quantum numbers of the vacuum. The experimental signatures of the diffraction consist in particular kinematic configurations of the final states: the presence of nonexponentially suppressed large rapidity gaps and/or the presence of the intact leading particles. The diffractive processes

became an important tool in understanding many interesting aspects of QCD such as low-x structure of the proton, the behavior of QCD in the high density regime.

Significant progress in understanding diffraction has been made at the Tevatron $p\bar{p}$ colliders. The CDF and D0 collaborations contributed extensively,[104–109] by studying a wide variety of diffractive processes at three different center-of-mass energies: 630 GeV, 1800 GeV — Run I of Tevatron and 1960 GeV — Run II. Some important results include the observation of QCD factorization breakdown in hard single diffractive processes, the discovery of large rapidity gaps between two jets, and the study of diffractive structure function in double pomeron exchange dijet events.

6.3.1. *Hard single diffraction*

The signature of single diffractive (SD) dissociation at the Tevatron is either a forward rapidity gap along the direction of one of the initial particles, or a presence of leading particle, antiproton, with $\xi < 0.1$. The process $\bar{p}p \to \bar{p}X$, which can be described by assuming that a pomeron is emitted by the incident antiproton and undergoes a hard scattering with the proton, is an ideal reaction to study the partonic content of the pomeron, and the diffractive structure function. The high energies of the Tevatron collider allows the study of diffraction in terms of perturbative QCD, i.e. in the presence of a hard scale. These types of diffractive processes are called *hard diffraction* and were extensively studied in Run I.[109]

One of the important questions in hard diffraction is whether these type of processes obey QCD factorization, or in other words, whether the pomeron has a universal process independent diffractive parton structure function. Results from Run I[104–107] show that the rate of single diffractive relative to nondiffractive processes is lower by an order of magnitude than expectations from diffractive PDFs determined at HERA ep collider. This presents breakdown of QCD factorization in hard diffraction between Tevatron and HERA. This suppression was further studied by investigating diffractive structure function in diffractive dijet production in Run I[108] and continuing these studies in Run II[110] by comparing two samples of dijets events, diffractive (SD) triggered by the presence of an intact antiproton detected in the Roman Pot Spectrometer (RPS), and nondiffractive (ND). By taking the ratio of SD dijet rates to ND, which in a good approximation is the ratio of the diffractive to the known proton structure function, the diffractive structure function can be extracted. The dependence of diffractive structure function on the average value of mean dijet E_T, Q^2 was studied. Figure 32(a) shows the ratio of the single diffractive dijet event rate to those of nondiffractive dijet events as a function of x_{BJ}, the Bjorken-x of the struck parton of the antiproton. In the range of $100 < Q^2 < 100,000\,\text{GeV}^2$ no significant Q^2 dependence is observed.

In addition, the t-distribution was measured for both soft and hard single diffractive processes, see Fig. 32(b). The slope of the distribution shows no dependence on the Q^2 of the process; for both soft and hard samples it is very similar. For

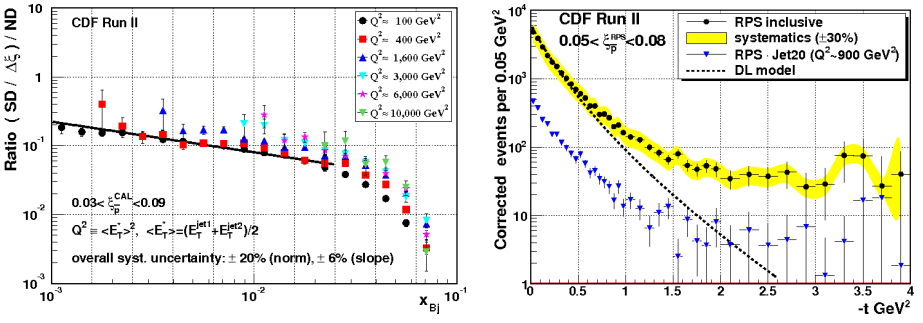

(a) (b)

Fig. 32. (a) The ratio of diffractive to nondiffractive dijet event rates as a function of x_{Bj} (momentum fraction of parton in the antiproton) for different values of Q^2 equal to the square of the mean dijet transverse energy E_T; (b) measured t distribution for two type of events (circles) soft single diffractive inclusive events and hard single diffractive (triangles) events triggered by presence of at least one jet with $E_T > 20$ GeV. The curve represents the distribution expected for soft SD in the Donnachie–Landshoff (DL) model.

low-t values, experimental results are well described by the curve based on predictions from the Donnachie–Landshoff model[111] for soft diffractive processes. High t values can be used to search for so-called "diffraction minimum" similar to the one observed for elastic scattering processes. However, the experimental data shows flat behavior and not enough discriminating resolution power.

Diffractive W/Z production is an important process for probing the quark content of the pomeron, since to leading order, the W/Z is produced through a quark, while gluon associated production is suppressed by a factor of α_S and can be identified by an additional jet. CDF studied diffractive W production in Run I[112] by using the rapidity gap signature of diffractive events. In Run II, events[113] were selected with the "intact leading antiproton" signature, where $\bar{p}$ is detected in the Roman Pot Spectrometers (RPS). The RPS allows very precise measurement of the fractional momentum loss of $\bar{p}$ (ξ), eliminating the problem of *gap survival probability*. The novel feature of the analysis, the determination of the full kinematics of the $W \to l\nu$ decay, is made possible by obtaining the neutrino ${E_T}^{\nu}$ from the missing E_T, $\not\!\!E_T$, and η_ν from the formula $\xi^{\rm RPS} - \xi^{\rm cal} = (\not\!\!E_T/\sqrt{s})\exp(-\eta_\nu)$, where $\xi^{\rm RPS}$ is the true ξ measured in RPS and $\xi^{\rm cal} = \sum_{i({\rm towers})} (E_T^i/\sqrt{s})\exp(-\eta^i)$. The fractions of diffractive W and Z events are measured to be $[0.97 \pm 0.05({\rm stat.}) \pm 0.11({\rm syst.})]\%$ and $[0.85 \pm 0.20({\rm stat.}) \pm 0.11({\rm syst.})]\%$ for the kinematic range $0.03 < \xi < 0.10$ and $|t| < 1\,{\rm GeV}$. The measured diffractive W fraction is consistent with the Run I CDF result[112] when corrected for the ξ and t ranges.

6.3.2. *Central exclusive production*

Central exclusive production, defined as the class of reactions $p + \bar{p} \to p + X + \bar{p}$, where the colliding particles emerge intact and a produced state, X, is fully

measured, has been the subject of much interest recently, particularly at large $\sqrt{s}$ where the rapidity range $\Delta y_{\text{total}} = 2 \times \ln \sqrt{s}/m_p = 15.3$ at the Tevatron allows the possibility of large rapidity gaps produced between state X and proton and antiproton. There are three production mechanisms responsible for this processes: $\gamma\gamma \to X$, $\gamma I\!P \to X$, and $I\!P I\!P \to X$, the so-called Double Pomeron Exchange (DPE). The first two processes were observed at CDF for the first time and will be discussed later.

CDF made an observation of exclusive dijet production[114] by studying events triggered by the intact leading antiproton on one side and a large rapidity gap in the proton direction. Although the $\xi_{\bar{p}}$ variable can be measured directly from the RPS information, ξ_p can be calculated by summing information from all the observed particles in the detector, $\xi_p = (1/\sqrt{s}) \sum E_T^i e^{\eta^i}$.

The exclusive dijet production was first studied by CDF in Run I data and a limit of $\sigma_{\text{excl}} < 3.7\,\text{nb}$ (95% CL) was placed.[115] This study was continued in Run II when the observation of the exclusive dijet production was reported.[114] The exclusive signal is extracted using the dijet mass fraction method: the ratio $R_{jj} \equiv M_{jj}/M_X$ of the dijet mass M_{jj} to the total mass M_X of the final state is formed and used to discriminate between the signal of exclusive dijets, defined as $R_{jj} > 0.8$, and the background of inclusive DPE dijets, expected to have a continuous distribution concentrated at lower R_{jj} values. The measured cross-sections, see Fig. 33, are consistent with KMR predictions by Khoze *et al.*.[116] The D0 collaboration extended the study of exclusive dijets into the highest mass states by presenting evidence[118] for diffractive exclusive dijet production with an invariant dijet mass M_{jj} greater than 100 GeV.

Another central exclusive process proceeding through the double pomeron exchange mechanism is exclusive diphoton production $p\bar{p} \to p\gamma\gamma\bar{p}$. CDF has performed a search for exclusive $\gamma\gamma$ in combination with the search for CEP e^+e^-.[119]

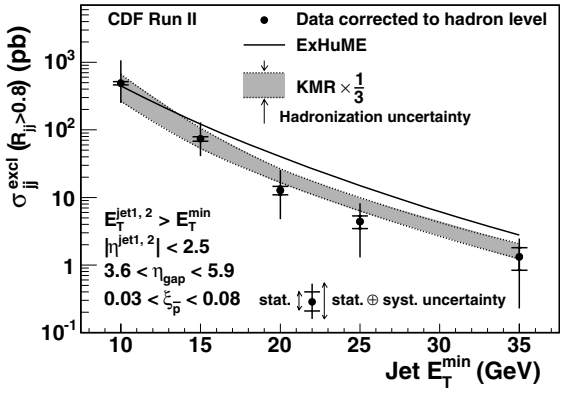

Fig. 33. Exclusive cross-section for events with two jets of $E_{T\text{jet}} > 10\,\text{GeV}$ with $R_{jj} > 0.8$ compared with ExHuME,[117] event generator based on perturbative calculations of Ref. 116, (solid curve) and with the LO analytical calculation KMR.

The analysis techniques were identical — to require absolutely empty detectors by triggering on very large forward rapidity gaps on both sides, except for two photon (electron) candidates. In contrast to exclusive diphoton search, where the theoretical predictions vary significantly for different models, central exclusive electron–positron production is a QED process with a well known cross-section, so while reporting an observation of exclusive electron–positron production in hadron–hadron collisions the CDF collaboration was able to validate the method for exclusive diphoton searches. The initial search for exclusive $\gamma\gamma$ production[120] using $532\,\mathrm{pb}^{-1}$ of data resulted in finding three candidate events and placing a limit. New analysis[121] utilized $1.11\,\mathrm{fb}^{-1}$ of data by selecting events with two electromagnetic showers, each with $E_T > 2.5\,\mathrm{GeV}$ and pseudorapidity $|\eta| < 1.0$ while requiring no other particles detected in the rest of the detector in pseudorapidity range from -7.4 to $+7.4$. The observed 43 candidate events have the kinematic properties expected for exclusive $\gamma\gamma$ production, see Fig. 34. This result constitutes the first observation of exclusive diphoton production in hadron–hadron collisions. The corresponding cross-section of $\sigma_{\gamma\gamma,\mathrm{excl}} = 2.48^{+0.40}_{-0.35}(\mathrm{stat})^{+0.40}_{-0.51}(\mathrm{syst})$ pb is in agreement with the theoretical predictions, where dependence on low-x gluon density contributes to significant uncertainty due to the choice of PDFs.

CDF II also studied dimuon production,[122] when the event signature requires two oppositely charged central muons, and either no other particles (large forward rapidity gaps), or one additional photon detected. Within the kinematic region $|\eta_\mu| < 0.6$ and $M_{\mu\mu} \in [3.0, 4.0]\,\mathrm{GeV}$, there are 402 events with no electromagnetic shower, see the $M_{\mu\mu}$ spectrum in Fig. 34(a).

The J/ψ and $\psi(2S)$ are prominent, so the exclusive vector meson production expected for the elastic photoproduction $\gamma + p \to J/\psi(\psi(2S)) + p$ is observed for the first time in hadron–hadron collisions. The obtained cross-sections $d\sigma/dy_{y=0}(J/\psi) = 3.92 \pm 0.25(\mathrm{stat}) \pm 0.52(\mathrm{syst})$ nb and for $\psi(2S) 0.53 \pm 0.09(\mathrm{stat}) \pm 0.10(\mathrm{syst})$ nb agree with the predictions,[123] while ratio $R = \sigma(\psi(2S))/\sigma(J/\psi) = 0.14 \pm 0.05$ is in agreement with the HERA value[124] of 0.166 ± 0.012 at similar $\sqrt{\gamma p}$. By requiring one EM shower with $E_T^{\mathrm{EM}} > 80\,\mathrm{MeV}$ in addition to the requirement mentioned above, we are able to measure χ_{c0} production. Allowing the EM tower causes a large increase (+66 events) in the J/ψ peak and minor change (+1 event) in the $\psi(2S)$ peak. After correcting for background, efficiencies, and the branching fraction, we observe $\chi_{c0} \to J/\psi + \gamma$ production for the first time in hadron–hadron collisions and obtain a cross-section for exclusive χ_{c0} production of $75 \pm 10(\mathrm{stat}) \pm 10(\mathrm{syst})$ nb, which is compatible with the theoretical predictions.[125]

In addition CDF performed a search for exclusive Z boson production.[126] No exclusive $Z \to l^+ l^-$ candidates were observed. The first upper limit on the exclusive Z cross-section in hadron collisions, $\sigma_{\mathrm{excl}}(Z) < 0.96\,\mathrm{pb}$ at 95% confidence level was placed.

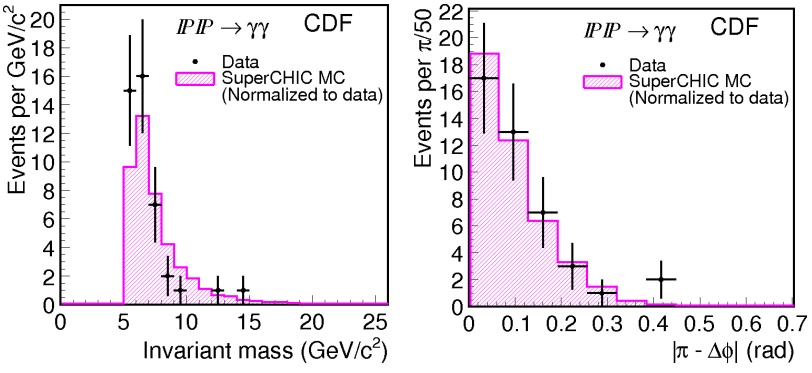

(a) (b)

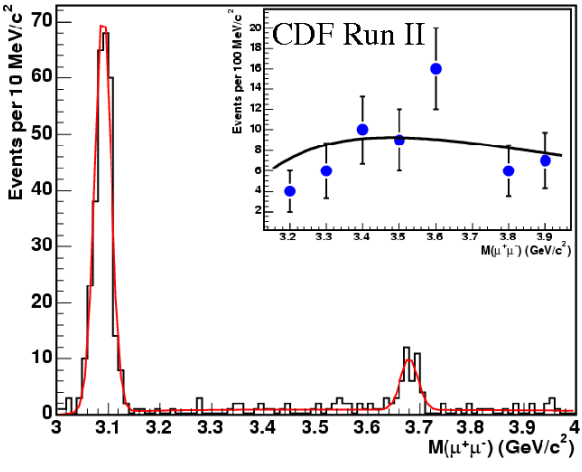

(c)

Fig. 34. (a) Invariant mass of exclusive photon pair events compared to MC; (b) azimuthal angle difference (from back-to-back) between the exclusive photons compared to MC; (c) mass, $M_{\mu\mu}$ of exclusive dimuon events, with no EM shower, (histogram) together with a fit to two Gaussians for the J/ψ and $\psi(2S)$, and a QED continuum. All three shapes are predetermined, with only the normalizations floating. Inset: Data above the J/ψ and excluding $3.65 < M_{\mu\mu} < 3.75\,\text{GeV}$ ($\psi(2S)$) with the fit to the QED spectrum times acceptance (statistical uncertainties only).

6.4. *Study of double parton interactions*

The CDF and D0 collaborations comprehensively studied the phenomenon of MPI events in a series of Run I and Run II measurements. The events with double parton (DP) scattering provide insight into the spatial distribution of partons in the colliding hadrons. They can be also a background to many rare processes, especially with multijet final state.

In Run I, CDF collaboration studied DP event using four-jet[127] and $\gamma + 3$[128] events. The observed fraction of DP events is found to be much higher in the $\gamma + 3$

final state (about 57%) than in the four-jet events (about 6%). Both these analyses measured the so-called effective cross-section, $\sigma_{\rm eff}$, that characterizes rates of the DP events, e.g. $\sigma_{\rm DP}^{\gamma j,jj} = \sigma^{\gamma j}\sigma^{jj}/\sigma_{\rm eff}$. This parameter is tightly related with the parton spatial distribution (see e.g. Ref. 129).

D0 has studied the DP events in $\gamma + 3$ jet final state,[130] in which two pairs of partons undergo two hard interactions in a single $p\bar{p}$ collision. D0 measured $\sigma_{\rm eff}$, and found it to be $\sigma_{\rm eff} = 16.4 \pm 0.3({\rm stat}) \pm 2.3({\rm syst})$. It is in agreement with the previous CDF result,[128] $\sigma_{\rm eff} = 14.5 \pm 1.7({\rm stat})^{+1.7}_{-2.3}({\rm syst})$, as well as with $\sigma_{\rm eff} = 12.1 \pm 10.7^{+10.7}_{-5.4}$.[128]

D0 collaboration has also tested a dependence of the effective cross-section on the initial quark flavor using the $\gamma + 3$-jet and $\gamma + b/c$ jet + 2 jet events with $p_T^{\gamma} > 26\,{\rm GeV}$ with inclusive and heavy flavor leading jet.[131] The effective cross-sections are found to be $\sigma_{\rm eff}^{\rm incl} = 12.7 \pm 0.2({\rm stat}) \pm 1.3({\rm syst})$ mb and $\sigma_{\rm eff}^{\rm HF} = 14.6 \pm 0.6({\rm stat}) \pm 3.2({\rm syst})$ mb for the two event types, respectively. This is the first measurement of $\sigma_{\rm eff}$ with heavy flavor jets in the final state. Due to the significant dominance of the Compton-like process $qg \to q\gamma$, one can conclude that there is no evidence for a dependence of $\sigma_{\rm eff}$ on the initial parton flavor. The plot (a) of Fig. 35 shows the ΔS distribution in the data, DP and single parton (SP) models, and the sum of the DP and SP contributions weighted with their fractions. Here the variable ΔS is defined as an azimuthal angle between the p_T vectors of two object pairs (γ + jet and jet + jet) in $\gamma + 3$ jet events. The found DP fractions vary within about 17–20%. The plot (b) summarizes the published world measurements (AFS, UA2, CDF, D0, ATLAS and CMS experiments) of the effective cross-section.

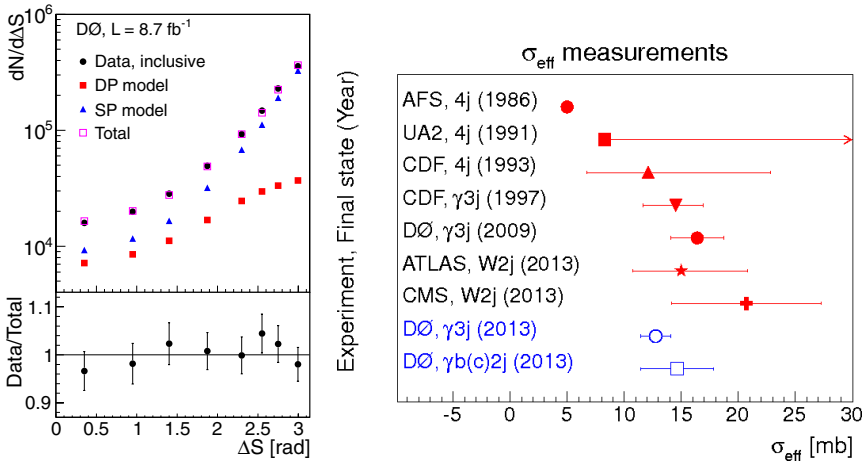

(a) (b)

Fig. 35. (a) The ΔS distribution in the data, DP and SP models, and the sum of the DP and SP contributions weighted with their fractions ("Total"). (b) Existing measurements of effective cross-section, $\sigma_{\rm eff}$, compared with result presented here (AFS: no uncertainty is reported; UA2: only a lower limit is provided).

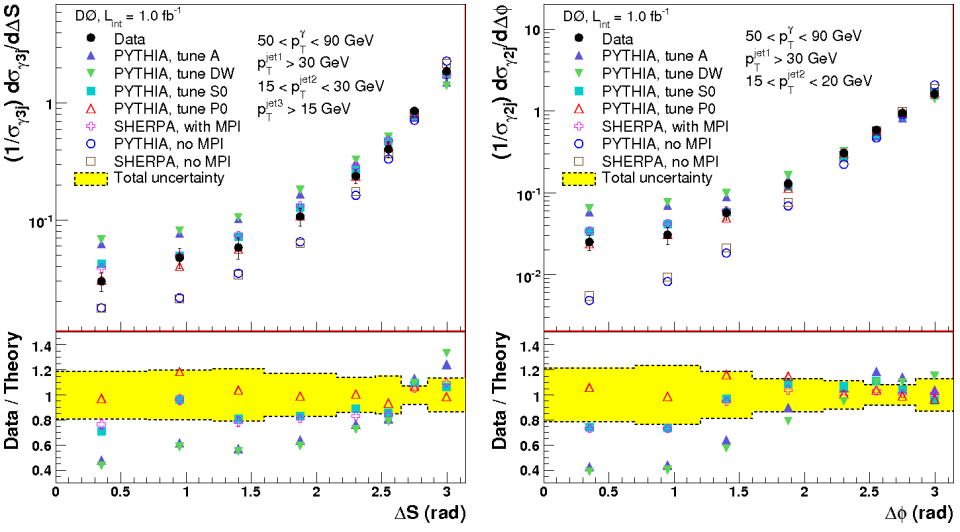

(a) (b)

Fig. 36. (a) Normalized differential cross-section in the $\gamma + 3\text{-jet} + \text{X}$ events, $(1/\sigma_{\gamma 3j})\sigma_{\gamma 3j}/d\Delta S$, in data compared to Monte Carlo models and the ratio of data over theory, only for models including MPI, in the range $15 < p_T^{\text{jet}2} < 30\,\text{GeV}$. (b) Normalized differential cross-section in $\gamma + 2\text{-jet} + \text{X}$ events, $(1/\sigma_{\gamma 2j})\sigma_{\gamma 2j}/d\Delta\phi$, in data compared to Monte Carlo models and the ratio of data over theory, only for models including MPI, in the range $15 < p_T^{\text{jet}2} < 20\,\text{GeV}$.

To tune MPI models, D0 also measured differential cross-sections for the ΔS variable in the three p_T bins of the 2nd jet p_T.[131,132] Comparison of data with a few MPI and two "no MPI" models are shown in Fig. 36. One can see that data clearly contain DP events and favor more Perugia MPI tunes.[16]

D0 collaboration has also studied recently the double J/ψ events produced due to DP interactions[133] with a dominated $gg \to J/\psi J/\psi$ production mechanism in each of the DP scatterings. Using DP events with a fraction of $f_{\text{DP}} = 0.30 \pm 0.10$, the effective cross-section has been estimated as $\sigma_{\text{eff}}^{JJ} = 5.0 \pm 0.5(\text{stat}) \pm 2.7(\text{syst})\,\text{mb}$.

7. Summary and Conclusions

In this short review, we presented main measurements and studies of the QCD processes performed by CDF and D0 experiments in Run II, for the data taking period from April 2002 to September 2011 (some Run I results are also briefly mentioned). These processes can be roughly split into those which are typically described in the framework of perturbative QCD, and those which are treated using phenomenological QCD models.

The measurements of the first type with jet final state are used to tune the gluon distribution at parton momentum fractions $x \gtrsim 0.2$, test running of α_s for momentum transfers up to 400 GeV and extract a precise integrated value $\alpha_s(m_Z) = 0.1161^{+0.0041}_{-0.0048}$, impose limits on some new phenomena which were

expected at high energies (e.g. excited quark, axigluon, technicolor models, W', and Z' productions). Measurements with photons provided a valuable input for tuning gluon PDFs at low x, soft-gluon resummations, and contributions from the parton-to-photon fragmentation processes, check a wide variety of approaches used to predict the differential $\gamma +$ (heavy flavor) jet and diphoton cross-sections. Numerous studies of $W/Z +$ jets productions allowed extensive tests and tuning pQCD NLO and Monte Carlo event generators, which have been used to predict backgrounds for Higgs boson production and searches for new phenomena at the Tevatron and LHC.

A broad physics program dedicated to studying soft strong interactions resulted in a bulk of interesting results. A series of minimum bias events studies allows tuning the nonperturbative QCD models which are used to describe underlying events and hadronization effects. Studies of MPI phenomenon at high p_T regime constrain existing MPI models, parton spatial densities inside a nucleon, and tune Monte Carlo event generators. Measurements of diffractive and elastic cross-sections test low-x structure of the proton and constrain many phenomenological models.

The obtained results affected a variety of models describing strong interactions between partons, may suggest directions of following studies, and compose a valuable legacy for other ongoing and future experiments and input for theoretical models.

Acknowledgments

Authors would like to than K. Anwar Bhatti and Robert Hirosky for useful comments and discussions. We thank the Fermilab staff and technical staffs of the participating institutions for their vital contributions. We acknowledge support from the DOE and NSF (USA), ARC (Australia), CNPq, FAPERJ, FAPESP and FUNDUNESP (Brazil), NSERC (Canada), NSC, CAS and CNSF (China), Colciencias (Colombia), MSMT and GACR (Czech Republic), the Academy of Finland, CEA and CNRS/IN2P3 (France), BMBF and DFG (Germany), DAE and DST (India), SFI (Ireland), INFN (Italy), MEXT (Japan), the KoreanWorld Class University Program and NRF (Korea), CONACyT (Mexico), FOM (Netherlands), MON, NRC KI and RFBR (Russia), the Slovak R&D Agency, the Ministerio de Ciencia e Innovacion, and Programa ConsoliderIngenio 2010 (Spain), The Swedish Research Council (Sweden), SNSF (Switzerland), STFC and the Royal Society (United Kingdom), the A.P. Sloan Foundation (USA) and the EU community Marie Curie Fellowship contract 302103.

References

1. A. Bhatti and D. Lincoln, *Ann. Rev. Nucl. Part. Sci* **60** (2010).
2. G. C. Blazey *et al.*, in *Proc. Workshop: QCD and Weak Boson Physics in Run* II, eds. U. Baur, R. K. Ellis and D. Zeppenfeld, Batavia, Illinois (2000), p. 47.
3. D0 Collab. (V. M. Abazov *et al.*), *Phys. Rev. Lett.* **101**, 062001 (2008); *Phys. Rev. D* **85**, 052006 (2012).

4. CDF Collab. (A. Abulencia *et al.*), *Phys. Rev. D* **74**, 071103(R) (2006).
5. CDF Collab. (A. Abulencia *et al.*), *Phys. Rev. D* **75**, 092006 (2007).
6. D0 Collab. (V. M. Abazov *et al.*), *Phys. Lett. B* **693**, 531 (2010).
7. A. D. Martin *et al.*, *Eur. Phys. J. C* **63**, 189 (2009).
8. J. Pumplin *et al.*, *J. High Energy Phys.* **07**, 012 (2002).
9. D0 Collab. (V. M. Abazov *et al.*), **704**, 434 (2011).
10. R. D. Ball *et al.*, *Nucl. Phys. B* **849**, 296 (2011).
11. S. Alekhin *et al.*, *Phys. Rev. D* **81**, 014032 (2010).
12. H. L. Lai *et al.*, *Phys. Rev. D* **82**, 074024 (2010).
13. H1 and ZEUS Collab. (F. D. Aaron *et al.*), *J. High Energy Phys.* **01**, 109 (2010).
14. D0 Collab. (V. M. Abazov *et al.*), *Phys. Lett. B* **720**, 6 (2013).
15. T. Gleisberg *et al.*, *J. High Energy Phys.* **02**, 007 (2009).
16. T. Sjöstrand, S. Mrenna and P. Z. Skands, *J. High Energy Phys.* **05**, 026 (2006).
17. D0 Collab. (V. M. Abazov *et al.*), *Phys. Rev. Lett.* **94**, 221801 (2005).
18. The PYTHIA parameter PARP(67) was increased from the current default of 1.0 to 4.0 which was the default before version 6.138.
19. D0 Collab. (V. M. Abazov *et al.*), *Phys. Lett. B* **712**, 212 (2013).
20. D0 Collab. (V. M. Abazov *et al.*), *Phys. Rev. D* **80**, 111107 (2009).
21. CDF Collab. (T. Affolder *et al.*), *Phys. Rev. Lett.* **88**, 042001 (2002).
22. H1 and ZEUS Collab. (C. Glasman), *J. Phys. Conf. Ser.* **110**, 022013 (2008).
23. D0 Collab. (V. M. Abazov *et al.*), *Phys. Lett. B* **718**, 56 (2012).
24. S. Bethke, *Eur. Phys. J. C* **64**, 689 (2009).
25. G. Dissertori *et al.*, *J. High Energy Phys.* **08**, 036 (2009).
26. D0 Collab. (V. M. Abbott *et al.*), *Phys. Rev. D* **65**, 052008 (2002).
27. CDF Collab. (T. Aaltonen *et al.*), *Phys. Rev. D* **85**, 091101 (2012).
28. CDF Collab. (D. Acosta *et al.*), *Phys. Rev. D* **71**, 112002 (2005).
29. CDF Collab. (T. Aaltonen *et al.*), *Phys. Rev. D* **78**, 072005 (2008).
30. CDF Collab. (T. Aaltonen *et al.*), *Phys. Rev. D* **72**, 112002 (2009).
31. D0 Collab. (V. M. Abazov *et al.*), *Phys. Rev. Lett.* **103**, 191803 (2009).
32. N. Arkani-Hamed, S. Dimopoulos and G. R. Dvali, *Phys. Lett. B* **429**, 263 (1998).
33. D. Atwood, S. Bar-Shalom and A. Soni, *Phys. Rev. D* **62**, 056008 (2000).
34. K. R. Dienes, E. Dudas and T. Gherghetta, *Nucl. Phys.* **B537**, 47 (1999).
35. CDF Collab. (F. Abe *et al.*), *Phys. Rev. Lett.* **73**, 2662 (1994); CDF Collab. (D. Acosta *et al.*), *Phys. Rev. D* **65**, 112003 (2002); D0 Collab. (S. Abachi *et al.*), *Phys. Rev. Lett.* **77**, 5011 (1996); D0 Collab. (B. Abbott *et al.*), *Phys. Rev. Lett.* **84**, 2786 (2000); D0 Collab. (V. M. Abazov *et al.*), *Phys. Rev. Lett.* **87**, 2518 (2001).
36. D0 Collab. (V. M. Abazov *et al.*), *Phys. Lett. B* **151**, 639 (2006).
37. CDF Collab. (T. Aaltonen *et al.*), *Phys. Rev. D* **80**, 111106 (2009).
38. ATLAS Collab. (G. Aad *et al.*), *Phys. Lett. B* **706**, 150 (2011).
39. CMS Collab. (S. Chatrchyan *et al.*), *Phys. Rev. D* **84**, 052011 (2011).
40. D. Enterria and J. Rojo, *Nucl. Phys. B* **860**, 311 (2012).
41. J. F. Owens, *Rev. Mod. Phys.* **59**, 465 (1987).
42. D0 Collab. (V. M. Abazov *et al.*), *Phys. Rev. D* **88**, 072008 (2013).
43. S. Catani, M. Fontannaz, J.-P. Guillet and E. Pilon, *J. High Energy Phys.* **05**, 028 (2002).
44. J. Pumplin *et al.*, *Phys. Rev. D* **75**, 054029 (2007).
45. S. J. Brodsky, P. Hoyer, C. Peterson and N. Sakai, *Phys. Lett. B* **93**, 451 (1980).
46. D0 Collab. (V. M. Abazov *et al.*), *Phys. Lett. B* **714**, 32 (2012).
47. D0 Collab. (V. M. Abazov *et al.*), *Phys. Lett. B* **719**, 354 (2013).
48. CDF Collab. (T. Aaltonen *et al.*), *Phys. Rev. Lett.* **111**, 042003 (2013).

49. T. Stavreva and J. F. Owens, *Phys. Rev. D* **79**, 054017 (2009).
50. A. V. Lipatov, M. A. Malyshev and N. P. Zotov, *J. High Energy Phys.* **05**, 104 (2012).
51. C. Amsler, *Phys. Lett. B* **667**, 1 (2008); see Section 17.8.
52. LHCb Collab. (R. Aaij *et al.*), *J. High Energy Phys.* **06**, 141 (2012).
53. ATLAS Collab. (G. Aad *et al.*), *Phys. Rev. D* **85**, 052005 (2012).
54. D0 Collab. (V. M. Abazov *et al.*), submitted to *Phys. Lett. B*, arXiv:1405.3964 [hep-ex].
55. H. B. Hartanto and L. Reina, *Phys. Rev. D* **89**, 074001 (2014).
56. P. Nadolsky, C. Balazs, E. Berger and C.-P. Yuan, *Phys. Rev. D* **76**, 013008 (2007).
57. T. Binoth, J. Ph. Guillet, E. Pilon and M. Werlen, *Eur. Phys. J. C* **16**, 311 (2000).
58. D0 Collab. (V. M. Abazov *et al.*), *Phys. Lett. B* **690**, 108 (2010).
59. CDF Collab. (T. Aaltonen *et al.*), *Phys. Rev. Lett.* **110**, 101801 (2013).
60. D0 Collab. (V. M. Abazov *et al.*), *Phys. Lett. B* **725**, 6 (2013).
61. CDF Collab. (T. Aaltonen *et al.*), *Phys. Rev. D* **84**, 052006 (2011).
62. CMS Collab. (S. Chatrchyan *et al.*), *Eur. Phys. J. C* **74**, 3129 (2014); *J. High Energy Phys.* **01**, 133 (2012).
63. ATLAS Collab. (G. Aad *et al.*), *Phys. Rev. D* **85**, 012003 (2012).
64. CDF Collab. (F. Abe *et al.*), *Phys. Rev. Lett.* **79**, 4760 (1997).
65. CDF Collab. (F. Abe *et al.*), *Phys. Rev. Lett.* **67**, 2937 (1991).
66. CDF Collab. (F. Abe *et al.*), *Phys. Rev. Lett.* **77**, 448 (1996).
67. D0 Collab. (B. Abbott *et al.*), *Phys. Lett. B* **464**, 145 (1999).
68. D0 Collab. (S. Abachi *et al.*), *Phys. Rev. Lett.* **75**, 3226 (1995).
69. D0 Collab. (V. M. Abazov *et al.*), *Phys. Rev. D* **88**, 092001 (2013).
70. CDF Collab. (T. Aaltonen *et al.*), *Phys. Rev. D* **91**, 012002 (2015).
71. M. Rubin, G. P. Salam and S. Sapeta, *J. High Energy Phys.* **1009**, 084 (2010).
72. A. Denner, S. Dittmaier, T. Kasprzik and A. Muck, *J. High Energy Phys.* **1106**, 069 (2011).
73. CDF Collab. (T. Aaltonen *et al.*), *Phys. Rev. Lett.* **104**, 131801 (2010).
74. D0 Collab. (V. M. Abazov *et al.*), *Phys. Lett. B* **718**, 1314 (2013).
75. J. M. Campbell and R. K. Ellis, *Nucl. Phys. Proc. Suppl.* **205**, 10 (2010).
76. J. Alwall *et al.*, *J. High Energy Phys.* **1106**, 128 (2011).
77. CDF Collab. (T. Aaltonen *et al.*), *Phys. Rev. Lett.* **110**, 071801 (2013).
78. CDF Collab. (T. Aaltonen *et al.*), *Phys. Rev. D* **79**, 052008 (2009).
79. D0 Collab. (V. M. Abazov *et al.*), *Phys. Rev. D* **83**, 031105 (2011).
80. D0 Collab. (V. M. Abazov *et al.*), *Phys. Rev. D* **87**, 092010 (2013).
81. D0 Collab. (V. M. Abazov *et al.*), *Phys. Rev. Lett.* **112**, 042001 (2014).
82. C. P. Fong and B. R. Webber, *Phys. Lett. B* **229**, 289 (1989); **241**, 255 (1990); *Nucl. Phys. B* **355**, 54 (1991).
83. CDF Collab. (F. Abe *et al.*), *Phys. Rev. Lett.* **61**, 1819 (1988); CDF Collab. (D. Acosta *et al.*), *Phys. Rev. D* **65**, 072005 (2002).
84. CDF Collab. (T. Aaltonen *et al.*), *Phys. Rev. D* **82**, 119903 (2010).
85. CDF Collab. (T. Affolder *et al.*), *Phys. Rev. D* **65**, 092002 (2002).
86. CDF Collab. (T. Aaltonen *et al.*), *Phys. Rev. D* **82**, 034001 (2010).
87. CDF Collab. (T. Aaltonen *et al.*), *Phys. Rev. D* **86**, 012002 (2012).
88. CDF Collab. (T. Aaltonen *et al.*), *Phys. Rev. D* **88**, 092005 (2013).
89. Y. L. Dokshitzer, V. Khoze, A. Mueller and S. Troyan, *Basics of Perturbative QCD*, ed. by J. Tran Thanh Van (Editions Frontières, Gif-sur-Yvette, 1991).
90. Y. I. Azimov, Y. L. Dokshitzer, V. A. Khoze and S. I. Troyan, *Z. Phys. C* **27**, 65 (2985); **31**, 213 (1986).
91. A. Dasgupta and G. P. Salam, *J. Phys. G* **30**, R143 (2004).

92. OPAL Collab. (G. Alexander *et al.*), *Phys. Lett. B* **265**, 462 (1001); OPAL Collab. (P. H. Acton *et al.*), *Z. Phys. C* **58**, 387 (1993); OPAL Collab. (R. Akers *et al.*), *Z. Phys. C* **68**, 179 (1995); ALEPH Collab. (D. Buskulic *et al.*), *Phys. Lett. B* **346**, 389 (1995); OPAL Collab. (G. Alexander *et al.*), *Phys. Lett. B* **388**, 659 (1996); ALEPH Collab. (D. Buskulic *et al.*), *Phys. Lett. B* **384**, 353 (1996); DELPHI Collab. (P. Abreu *et al.*), *Z. Phys. C* **70**, 179 (1996); OPAL Collab. (K. Ackerstaff *et al.*), *Eur. Phys. J. C* **1**, 479 (1998); DELPHI Collab. (P. Abreu *et al.*), *Phys. Lett. B* **449**, 383 (1999); OPAL Collab. (G. Abbiendi *et al.*), *Eur. Phys. J. C* **11**, 217 (1999); SLD Collab. (Y. Iwasaki *et al.*), SLAC Report, Stanford, SLAC-R-95-460, 1995.
93. CDF Collab. (T. Affolder *et al.*), *Phys. Rev. Lett.* **87**, 211804 (2001); CDF Collab. (D. Acosta *et al.*), *Phys. Rev. D* **68**, 012003 (2003).
94. CDF Collab. (T. Aaltonen *et al.*), *Phys. Rev. D* **77**, 092001 (2008).
95. R. P. Ramos, *J. High Energy Phys.* **06**, 019 (2006); **09**, 014 (2006).
96. CDF Collab. (T. Aaltonen *et al.*), *Phys. Rev. Lett.* **102**, 232002 (2009).
97. F. Arleo, R. Perez-Ramos and B. Machet, *Phys. Rev. Lett.* **100**, 052002 (2008); F. Arleo, R. Perez-Ramos and B. Machet, *Phys. Rev. D* **78**, 014019 (2008).
98. CDF Collab. (T. Aaltonen *et al.*), *Phys. Rev. D* **83**, 112007 (2011).
99. A. Banfi, G. P. Salam and G. Zanderighi, *J. High Energy Phys.* **08**, 062 (2004).
100. CDF Collab. (F. Abe *et al.*), *Phys. Rev. D* **50**, 5518 (1994).
101. D0 Collab. (V. M. Abazov *et al.*), *Phys. Rev. D* **86**, 012009 (2012).
102. E710 Collab. (N. Amos *et al.*), *Phys. Lett. B* **247**, 127 (1990).
103. UA4 Collab. (M. Bozzo *et al.*), *Phys. Lett. B* **155**, 197 (1985).
104. CDF Collab. (F. Abe *et al.*), *Phys. Rev. Lett.* **79**, 2636 (1997).
105. CDF Collab. (F. Abe *et al.*), *Phys. Rev. Lett.* **78**, 2698 (1997).
106. CDF Collab. (T. Affolder *et al.*), *Phys. Rev. Lett.* **84**, 232 (2000).
107. CDF Collab. (T. Affolder *et al.*), *Phys. Rev. Lett.* **87**, 241802 (2001).
108. CDF Collab. (T. Affolder *et al.*), *Phys. Rev. Lett.* **84**, 5043 (2000).
109. CDF Collab. (F. Abe *et al.*), *Phys. Rev. D* **50**, 5535 (1994); D0 Collab. (S. Abachi *et al.*), *Phys. Rev. Lett.* **72**, 2332 (1994); D0 Collab. (S. Abachi *et al.*), *Phys. Rev. Lett.* **76**, 734 (1996); CDF Collab. (F. Abe *et al.*), *Phys. Rev. Lett.* **81**, 5278 (1998); CDF Collab. (F. Abe *et al.*), *Phys. Rev. Lett.* **80**, 1156 (1998); D0 Collab. (S. Abachi *et al.*), *Phys. Lett. B* **440**, 189 (1998); CDF Collab. (D. Acosta *et al.*), *Phys. Rev. Lett.* **88**, 151802 (2002); D0 Collab. (V. M. Abazov *et al.*), *Phys. Lett. B* **531**, 52 (2002); D0 Collab. (V. M. Abazov *et al.*), *Phys. Lett. B* **574**, 169 (2003).
110. CDF Collab. (T. Aaltonen *et al.*), *Phys. Rev. D* **86**, 032009 (2012).
111. A. Donnachie and P. Landshoff, *Phys. Lett. B* **518**, 63 (2001).
112. CDF Collab. (T. Aaltonen *et al.*), *Phys. Rev. Lett.* **78**, 2698 (1997).
113. CDF Collab. (T. Aaltonen *et al.*), *Phys. Rev. D* **82**, 112004 (2010).
114. CDF Collab. (T. Aaltonen *et al.*), *Phys. Rev. D* **77**, 052004 (2008).
115. CDF Collab. (T. Affolder *et al.*), *Phys. Rev. Lett.* **85**, 4215 (2000).
116. V. A. Khoze, A. D. Martin and M. G. Ryskin, *Eur. Phys. J. C* **14**, 525 (2000); V. A. Khoze, A. D. Martin and M. G. Ryskin, arXiv:0705.2314.
117. J. Monk and A. Pilkington, *Comput. Phys. Commun.* **175**, 232 (2006).
118. D0 Collab. (V. M. Abazov *et al.*), *Phys. Lett. B* **705**, 193 (2011).
119. CDF Collab. (T. Aaltonen *et al.*), *Phys. Rev. Lett.* **98**, 112001 (2007).
120. CDF Collab. (T. Aaltonen *et al.*), *Phys. Rev. Lett.* **99**, 242002 (2007).
121. CDF Collab. (T. Aaltonen *et al.*), *Phys. Rev. Lett.* **108**, 081801 (2012).
122. CDF Collab. (T. Aaltonen *et al.*), *Phys. Rev. Lett.* **102**, 242001 (2009).
123. S. Klein and J. Nystrand, *Phys. Rev. Lett.* **92**, 142003 (2004); L. Motyka and G. Watt, *Phys. Rev. D* **78**, 014023 (2008); W. Schäfer and A. Szczurek, *Phys. Rev. D*

76, 094014 (2007); V. P. Goncalves and M. V. T. Machado, *Eur. Phys. J. C* **40**, 519 (2005).
124. H. Jung, *Acta Phys. Pol. Supp.* **1**, 531 (2008), and references therein.
125. V. A. Khoze *et al.*, *Eur. Phys. J. C* **35**, 211 (2004); V. A. Khoze *et al.*, *Eur. Phys. J. C* **19**, 599(E) (2001); F. Yuan, *Phys. Lett. B* **510**, 155 (2001); A. Bzdak, *Phys. Lett. B* **619**, 288 (2005).
126. CDF Collab. (T. Aaltonen *et al.*), *Phys. Rev. Lett.* **102**, 222002 (2009).
127. CDF Collab. (F. Abe *et al.*), *Phys. Rev. D* **47**, 4857 (1993).
128. CDF Collab. (F. Abe *et al.*), *Phys. Rev. D* **56**, 3811 (1997).
129. G. Calucci and D. Treleani, *Phys. Rev. D* **60**, 054023 (1999).
130. D0 Collab. (V. M. Abazov *et al.*), *Phys. Rev. D* **81**, 052012 (2010).
131. D0 Collab. (V. M. Abazov *et al.*), *Phys. Rev. D* **83**, 052008 (2013).
132. D0 Collab. (V. M. Abazov *et al.*), *Phys. Rev. D* **89**, 072006 (2014).
133. D0 Collab. (V. M. Abazov *et al.*), *Phys. Rev. Lett.* **90**, 111101(R) (2014).